Extensions of the Standard Model Scalar Sector and Constraints From Colliders and Cosmology

Ville Vaskonen

UNIVERSITY OF JYVÄSKYLÄ
DEPARTMENT OF PHYSICS

Master's Thesis
Supervisor: Kimmo Tuominen

Abstract

In this thesis we study the Higgs sector of the Standard Model and compare it to the latest data from the LHC and Tevatron experiments. Then we consider two extensions of the Higgs sector. First we extend the Standard Model Higgs sector with one real SU(2) singlet and then we consider two-Higgs-doublet model and extend also it with one real singlet. In both extensions the singlet scalar is considered as a potential dark matter candidate. We find that the parameter space of the so called two-Higgs-doublet-inert-singlet model includes regions which could provide a dark matter candidate which constitutes significant amount of the total dark matter mass density.

Contents

Chapter 1

Introduction

Nowadays the understanding of the elementary particle physics is largely based on the Standard Model (SM). The success of the SM has been astonishing. It predicted the existence of the heaviest quarks (charm [1] , bottom [2] and top [3]) and gauge bosons Z, W [4, 5] before they were experimentally observed. In the last few decades it has been tested in many experiments and shown to successfully describe the high energy physics phenomena. For a long time the Higgs sector has been the only unverified part of the SM. However, the newly found neutral boson [6, 7] seems to be well consistent with the SM Higgs boson.

Despite the great success we are not fully pleased with the SM. First of all there are some problems with the Higgs sector. The SM does not explain why the weak force is so much stronger than gravity. The central challenges in elementary particle physics today are Higgs physics, dark matter problem and baryon asymmetry problem. For some reason there seems to be much more matter than antimatter in the Universe. To explain the asymmetry one would need sufficient amount of CP violation in the elementary particle physics model. The SM does not offer enough CP violation and can not explain the baryon asymmetry. Moreover, measurements [8] have shown that only less than 5% of the energy density of the observable universe consists of ordinary baryonic matter. The rest of the matter-energy content is dark matter (27%) and dark energy (68%). The nature of dark matter is still one of the biggest mysteries in physics. New weakly interacting massive particles (WIMPs) are probably the most favorable candidates for the dark matter, but there are no WIMP candidates in the SM. Also the nature of dark energy is not understood, but we will ignore the dark energy problem in this thesis.

There is no way SM could explain the dark matter or the baryon asymmetry problem, thus we need to search for a model beyond the SM. In this thesis we will concentrate mainly on the dark matter problem, keeping in mind also the

baryon asymmetry problem. One way to approach the dark matter problem is to try to understand the physics of the Higgs sector. Extensions of the Higgs sector could provide dark matter candidates as well as sources for the CP violation which could explain the baryon asymmetry. We will consider two extensions of the Higgs sector: first we consider the SM Higgs sector with an additional real scalar singlet, and then we study the two-Higgs-doublet model with an additional real singlet. In both cases the singlet field is considered as a dark matter candidate. We constrain these models with Higgs decay data from the LHC and Tevatron experiments, and with the electroweak precision data. Moreover we calculate relic abundances of the dark matter particle candidates. We begin with the SM Higgs sector.

Chapter 2

The Standard Model Higgs sector

2.1 Electroweak symmetry breaking

The SM is a gauge theory, which describes fundamental particles and their electroweak and strong interactions. The gauge symmetry of the SM is $\mathrm{SU(3)_C} \times \mathrm{SU(2)_L} \times \mathrm{U(1)_Y}$. We will focus on the electroweak sector $\mathrm{SU(2)_L} \times \mathrm{U(1)_Y}$ introduced by Glashow, Weinberg and Salam [9, 10] . The gauge symmetry prevents us from adding mass terms for gauge bosons and fermions. In the SM masses are obtained through spontaneous symmetry breaking (SSB) [11, 12] , that via the Higgs mechanism gives masses to gauge bosons W and Z and leaves only $\mathrm{U(1)_{EM}}$ as a manifest symmetry of the vacuum. The idea of the Higgs mechanism is to introduce scalar fields and a scalar potential, which gives a non-zero vacuum expectation value (VEV) to one of the scalar fields, leading to massive gauge bosons, quarks and charged leptons through their couplings with the scalar fields.

In the SM the scalar sector consists of one SU(2) doublet (with hypercharge $Y = 1$)

$$\phi = \begin{pmatrix} \phi^+ \\ \phi^0 \end{pmatrix} . \tag{2.1}$$

The Lagrangian describing the scalar sector is

$$\mathcal{L}_{\mathrm{Higgs}} = (D_\mu \phi)^\dagger (D^\mu \phi) - V(\phi) , \tag{2.2}$$

where

$$D_\mu = \partial_\mu + ig\frac{\tau_j}{2}A^j_\mu + ig'\frac{Y}{2}B_\mu \tag{2.3}$$

is the covariant derivative and

$$V(\phi) = -\mu^2 \phi^\dagger \phi + \frac{\lambda}{4}(\phi^\dagger \phi)^2 \tag{2.4}$$

is the scalar potential. Due to hermiticity of the Lagrangian the parameters μ^2 and λ are real. Stability of the vacuum requires the potential to be bounded from below, which means that λ is positive. To obtain a non-zero minimum of the potential, which is essential in order to break the symmetry, we also take $\mu^2 > 0$. Then we choose a particular minimum

$$\langle\phi\rangle = \begin{pmatrix} 0 \\ \frac{v}{\sqrt{2}} \end{pmatrix} , \tag{2.5}$$

where $v = 2\mu/\sqrt{\lambda}$, so that the doublet ϕ acquires a VEV $\langle\phi\rangle$.

To find out the tree-level mass eigenstates we calculate the mass matrices,

$$M^2 = \left(\frac{\partial^2 V}{\partial\phi_j \partial\phi_k}\bigg|_{\phi=\langle\phi\rangle} \right) , \tag{2.6}$$

for charged and neutral scalar fields, and diagonalize them. In the SM the full mass matrix in the basis $\{\phi^+, \mathrm{Re}\,(\phi^0)\,, \mathrm{Im}\,(\phi^0)\}$ is

$$\begin{pmatrix} 0 & 0 & 0 \\ 0 & \frac{v^2\lambda}{2} & 0 \\ 0 & 0 & 0 \end{pmatrix} . \tag{2.7}$$

Hence, after the symmetry breaking we obtain one neutral massless scalar field $\mathrm{Im}\,(\phi^0)$ and two charged massless scalar fields $\phi^\pm$, which are the Goldstone bosons eaten by the gauge fields leading to massive gauge bosons Z and $W^\pm$, and one neutral massive scalar boson $\mathrm{Re}\,(\phi^0)$, which is the Higgs boson.

To see in detail how we get rid of the Goldstone bosons we write

$$\phi = \mathrm{e}^{-\mathrm{i}\eta_j\tau^j} \begin{pmatrix} 0 \\ \frac{1}{\sqrt{2}}(h+v) \end{pmatrix} , \tag{2.8}$$

where η_j and h are real scalar fields with VEVs $\langle\eta_j\rangle = 0 = \langle h\rangle$, and τ^j are the SU(2) generators. Now we transform to the so called unitary gauge by performing a $\mathrm{SU(2)_L}$ gauge transformation $U = \mathrm{e}^{\mathrm{i}\eta_j\tau^j}$. Expanding the Lagrangian of the Higgs sector $\mathcal{L}_{\mathrm{Higgs}}$ we get

$$\begin{aligned} \mathcal{L}_{\mathrm{Higgs}} = {} & \frac{1}{4}\partial^2 h^2 + \frac{1}{4}g^2 h^2 W^- W^+ + \frac{1}{2}g^2 hv W^- W^+ + \frac{1}{4}g^2 v^2 W^- W^+ \\ & + \frac{1}{8}(g^2+g'^2)h^2 Z^2 + \frac{1}{4}(g^2+g'^2)hvZ^2 + \frac{1}{8}(g^2+g'^2)v^2 Z^2 \\ & + \frac{h^4\lambda}{16} + \frac{1}{4}h^3 v\lambda + \frac{1}{4}h^2 v^2\lambda - \frac{v^4\lambda}{16} , \end{aligned} \tag{2.9}$$

where

$$W^{\pm} = \frac{1}{\sqrt{2}} \left(A^1 \mp i A^2 \right) \ , \tag{2.10}$$

and

$$\begin{pmatrix} Z \\ A \end{pmatrix} = \begin{pmatrix} \cos\theta_W & -\sin\theta_W \\ \sin\theta_W & \cos\theta_W \end{pmatrix} \begin{pmatrix} A^3 \\ B \end{pmatrix} \ . \tag{2.11}$$

The Weinberg angle θ_W is defined such that

$$g = \frac{e}{\sin\theta_W} \ , \quad g' = \frac{e}{\cos\theta_W} \tag{2.12}$$

in order to obtain the correct electron-photon and neutrino-photon interactions. From the equation (2.9) we can easily identify mass terms for W and Z bosons as well as for the Higgs boson h , and see that there are no Goldstone bosons.

The parameter v is attached by the Z boson mass

$$M_Z = \sqrt{g^2 + g'^2} v/2 \ , \tag{2.13}$$

which has a measured value $M_Z = 91.19\,\mathrm{GeV}$. For coupling constant values $g(M_Z) = 0.650$, $g'(M_Z) = 0.358$ we obtain $v \approx 246\,\mathrm{GeV}$. Now $\mu = v\sqrt{\lambda}/2$ so the only unknown parameter in the SM Higgs sector is λ or equivalently the mass of the Higgs boson $m_h^2 = v^2\lambda/2$.

SSB also leads to massive fermions through the Yukawa interactions

$$\mathcal{L}_{\text{Yukawa}} = \frac{Y_e}{2} \overline{\psi}^T_{l,L} \phi \psi_{e,R} + \frac{Y_u}{2} \overline{\psi}^T_{q,L} (-\mathrm{i}\tau_2 \phi) \psi_{u,R} + \frac{Y_d}{2} \overline{\psi}^T_{q,L} \phi \psi_{d,R} + \text{h.c.} \ . \tag{2.14}$$

After SSB the interactions of the Higgs boson with the gauge bosons and fermions are summarized by the Lagrangian

$$\begin{aligned} \mathcal{L}_{\text{int}} = & \frac{2M_W^2}{v} h W^+ W^- + \frac{M_Z^2}{v} h Z^2 + \frac{M_W^2}{v^2} h^2 W^+ W^- + \frac{M_Z^2}{2v^2} h^2 Z^2 \\ & - \sum_{\psi} \frac{m_\psi}{\sqrt{2}v} h \left(\overline{\psi}_L \psi_R + \text{h.c} \right) \ , \end{aligned} \tag{2.15}$$

where the sum is taken over charged leptons e, μ, τ and quarks u, d, s, c, b, t . Note that coupling of any massive particle to the Higgs boson is proportional to its mass, so the top quark has the strongest fermion-Higgs boson coupling.

2.2 Discovery of a new neutral boson at the LHC

One of the main goals of the Large Hadron Collider (LHC) has been to search for the SM Higgs boson in the proton-proton collisions. On July 4th 2012 ATLAS

and CMS collaborations announced that they had found a clear evidence of a neutral boson with mass of approximatively 125.7 GeV [6, 7] . The significance of the observation was 4.9σ (see appendix A for summary of statistics). Since then the significance has increased and is already more than 7σ . More recently also CDF and C0 collaborations have found similar evidences for the new boson from the Tevatron data [13] . Hence it is now obvious that there is a new neutral boson. The mass of the new particle can be obtained from the position of the observed peaks in the $h \to ZZ \to 4l$ and $h \to \gamma\gamma$ channels. Latest results for the mass of the new boson are $125.2 \pm 0.3(\text{stat.}) \pm 0.6(\text{syst.})$ from the ATLAS experiment [14] and $125.7 \pm 0.3(\text{stat.}) \pm 0.3(\text{syst.})$ from the CMS experiment [15] . Next we will look at the Higgs couplings and see whether the new boson is the SM Higgs boson.

2.3 LHC and Tevatron data fit

There are five dominant Higgs boson production channels in the proton-proton collisions in the mass range around 125 GeV in the SM. These production channels are presented in figure 2.1 and the corresponding cross-sections for $\sqrt{s} = 2, 7, 8\,\text{TeV}$ are collected in table 2.1 . Likewise, there are nine dominant Higgs decay channels which are presented in figure 2.2 corresponding to branching ratios presented in table 2.2 . The Higgs boson does not directly couple to photons, because it is neutral, so the leading order contribution to $h \to \gamma\gamma$ arises from the top and W loop diagrams. The $h \to WW$ and $h \to ZZ$ decay channels are followed by the decay of the gauge bosons to leptons. For the experiments, the most important decay channels are $h \to ZZ \to 4l$ ($l = e, \mu$) and $h \to \gamma\gamma$ due to the excellent mass resolution for the reconstructed $\gamma\gamma$ and $4l$ final states [16].

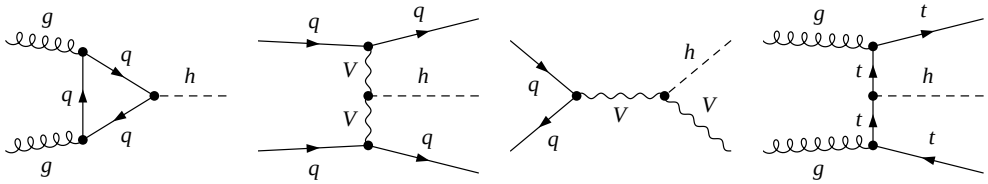

(a) ggF **(b)** VBF **(c)** VH **(d)** ttH

Figure 2.1. Dominating Higgs boson production channels in the SM.

Experimental collaborations give signal strength values for different decay

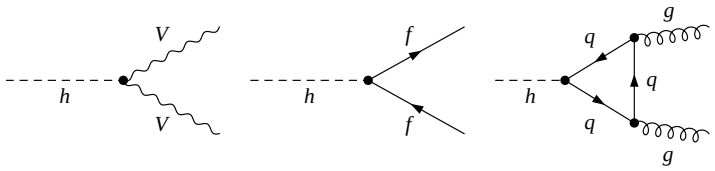

(a) $h \to VV$ **(b)** $h \to ff$ **(c)** $h \to gg$

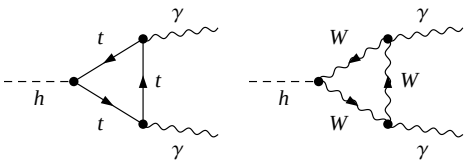

(d) $h \to \gamma\gamma$

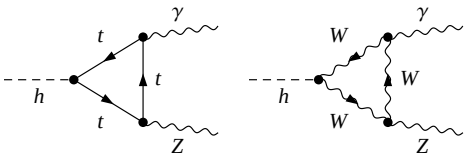

(e) $h \to Z\gamma$

Figure 2.2. Dominating Higgs boson decay channels in the SM.

channels of the Higgs[1]. The ATLAS and CMS collaborations have measured the signal strength for five different decay channels and from the Tevatron data we get signal strengths for three decay channels. Latest results are presented in table 2.3 . The LHC results are combined from experiments with center of mass energies $\sqrt{s} = 7\,\text{TeV}$ and $\sqrt{s} = 8\,\text{TeV}$. For the Tevatron results $\sqrt{s} = 2\,\text{TeV}$.

Let us see how the SM Higgs boson fits with the most recent results of the ATLAS, CMS and Tevatron experiments. Similar analysis for different models is done for example in references [21–25] . We consider modified Higgs couplings, where the couplings of the Higgs boson to fermions are multiplied by a factor a_f and to gauge bosons by a factor a_V . Hence we study an effective

[1]Henceforth we will refer the newly found neutral boson as the Higgs or the Higgs boson.

Table 2.1. Production cross-sections of the SM Higgs boson ($m_h = 125\,\text{GeV}$) for $\sqrt{s} = 8, 7, 2\,\text{TeV}$ [17, 18] .

	ggF	VBF	WH	ZH	ttH
$\sigma_{8\,\text{TeV}}(\text{pb})$	19.52	1.578	0.6966	0.3943	0.1302
$\sigma_{7\,\text{TeV}}(\text{pb})$	15.32	1.222	0.5729	0.3158	0.0863
$\sigma_{2\,\text{TeV}}(\text{pb})$	0.9493	0.0653	0.1295	0.0785	0.0043

Table 2.2. Decay branching ratios of the SM Higgs boson ($m_h = 125\,\text{GeV}$) [19].

	BR		BR		BR
$h \to bb$	$5.77{\cdot}10^{-1}$	$h \to \tau\tau$	$6.32{\cdot}10^{-2}$	$h \to \gamma\gamma$	$2.28{\cdot}10^{-3}$
$h \to WW$	$2.15{\cdot}10^{-1}$	$h \to cc$	$2.91{\cdot}10^{-2}$	$h \to Z\gamma$	$1.54{\cdot}10^{-3}$
$h \to gg$	$8.57{\cdot}10^{-2}$	$h \to ZZ$	$2.64{\cdot}10^{-2}$	$h \to \mu\mu$	$2.20{\cdot}10^{-4}$

Lagrangian density

$$\mathcal{L}_{\text{eff}} = a_V \frac{2M_W^2}{v} h W^+ W^- + a_V \frac{M_Z^2}{v} h Z Z - a_f \sum \frac{m_\psi}{v} h \overline{\psi}\psi \; . \tag{2.16}$$

We could also add for example an extra gauge boson W' with coupling $2a'_V m_{W'}^2/v$ to Higgs boson or a scalar boson S_0 with coupling $a_S m_{S_0}^2/v$ to the Higgs boson, but for our analysis here these are not important.

The signal strength corresponding to decay channel j is defined as

$$\mu_j = \frac{\sigma_{\text{tot}} \text{BR}_j}{\sigma_{\text{SMtot}} \text{BR}_{\text{SM}j}} \; , \tag{2.17}$$

where σ_{tot} and BR_j are the measured total production cross-section of the Higgs boson and branching ratio to the decay channel j , and $\sigma_{\text{SMtot}}, \text{BR}_{\text{SM}j}$ are

Table 2.3. Observed signals strengths $\mu_{obs,j}$ for different Higgs decay channels from the ATLAS [20], CMS [15] and Tevatron [18] experiments.

	ATLAS	CMS	Tevatron
ZZ	1.47 ± 0.38	0.91 ± 0.27	
$\gamma\gamma$	1.65 ± 0.34	1.11 ± 0.31	3.64 ± 2.78
WW	0.96 ± 0.30	0.76 ± 0.21	0.33 ± 0.86
$\tau\tau$	0.75 ± 0.69	1.10 ± 0.40	
bb	-0.40 ± 1.02	1.08 ± 0.59	1.98 ± 0.75

the corresponding values calculated from the SM. We can use the formula (2.17) also to calculate the signal strength values for any model just by replacing the nominator by the production cross-section and branching ratio calculated from the model. Note that for the SM $\mu_j = 1$ for all decay channels.

Next we use the formula (2.17) to calculate μ_j values corresponding to the Lagrangian (2.16) . Writing the branching ratio BR_j in terms of the decay width Γ_j and the total decay width $\Gamma_{\mathrm{tot}} = \sum_j \Gamma_j$,

$$\mathrm{BR}_j = \frac{\Gamma_j}{\Gamma_{\mathrm{tot}}} \ , \tag{2.18}$$

we get

$$\mu_j = \frac{\sigma_{\mathrm{tot}}}{\sigma_{\mathrm{SMtot}}} \frac{\Gamma_j}{\Gamma_{\mathrm{SM}j}} \left(\frac{\Gamma_{\mathrm{tot}}}{\Gamma_{\mathrm{SMtot}}} \right)^{-1} \ . \tag{2.19}$$

The total Higgs decay width in the SM is $\Gamma_{\mathrm{SMtot}} = 4.07$. It is useful to define

$$G_j = \frac{\Gamma_j}{\Gamma_{\mathrm{SM}j}} \ , \quad s_j = \frac{\sigma_j}{\sigma_{\mathrm{SM}j}} \ , \tag{2.20}$$

whereby

$$\frac{\Gamma_{\mathrm{tot}}}{\Gamma_{\mathrm{SMtot}}} = \sum_k G_k \mathrm{BR}_{\mathrm{SM}k} \ , \tag{2.21}$$

and

$$\mu_j = \left(\sum_l s_l \frac{\sigma_{\mathrm{SM}l}}{\sigma_{\mathrm{SMtot}}} \right) \left(\frac{G_j}{\sum_k G_k \mathrm{BR}_{\mathrm{SM}k}} \right) \ . \tag{2.22}$$

The k summations in the formulae (2.21) and (2.22) include the final states (ff,VV,gg,$\gamma\gamma$,Zγ) and the l summation in formula (2.22) includes the initial states (ggF,VBF,VH,ttH).

The only thing we need to do now is to find out s_j for different production channels and G_j for different decay channels of the Higgs boson. We take into account only the leading order interactions. By looking at the Feynman diagrams shown in figure 2.1 , and remembering that we modify the higgs-gauge boson interactions by a factor a_V and higgs-fermion interactions by a factor a_f , it is easy to see that

$$s_{\mathrm{ggF}} = a_f^2 \ , \ s_{\mathrm{VBF}} = a_V^2 \ , \ s_{\mathrm{WH}} = a_V^2 \ , s_{\mathrm{ZH}} = a_V^2 \ , \ s_{\mathrm{ttH}} = a_f^2 \ . \tag{2.23}$$

Similarly from the decay channel diagrams 2.2 we see that

$$\begin{gathered} G_{bb} = a_f^2 \ , \ G_{\tau\tau} = a_f^2 \ , \ G_{cc} = a_f^2 \ , \ G_{\mu\mu} = a_f^2 \ , \\ G_{WW} = a_V^2 \ , \ G_{ZZ} = a_V^2 \ , \ G_{gg} = a_f^2 \ , \ G_{Z\gamma} = a_V^2 \ . \end{gathered} \tag{2.24}$$

The $h \to \gamma\gamma$ decay channel is in turn more complicated, because top and W loop diagrams give contribution of the same order of magnitude. Hence we need to go to the amplitude level. By using the formulae given in [26] we write

$$\Gamma_{\gamma\gamma}(a_f, a_V) = \frac{\alpha^2 g^2 m_h^3}{1024\pi^3 M_W^2} \left| \frac{4}{3} a_f F_{1/2} + a_V F_1 \right|^2 , \tag{2.25}$$

where

$$\begin{aligned} F_{1/2} &= -2\frac{4m_t^2}{m_h^2}\left(1 + \left(1 - \frac{4m_t^2}{m_h^2}\right) f\left(\frac{4m_t^2}{m_h^2}\right)\right) , \\ F_1 &= 2 + 3\frac{4M_W^2}{m_h^2} + 3\frac{4M_W^2}{m_h^2}\left(2 - \frac{4M_W^2}{m_h^2}\right) f\left(\frac{4M_W^2}{m_h^2}\right) , \end{aligned} \tag{2.26}$$

and

$$f(\tau) = \begin{cases} \arcsin^2 \sqrt{\frac{1}{\tau}} , & \tau \geq 1 , \\ -\frac{1}{4}\left(\log\left(\frac{\sqrt{1-\tau}+1}{1-\sqrt{1-\tau}}\right) - \mathrm{i}\pi\right)^2 , & \tau < 1 . \end{cases} \tag{2.27}$$

Now using $\alpha = 7.30 \cdot 10^{-3}$, $g = 0.653$, $M_W = 80.4\,\mathrm{GeV}$ and $m_h = 125\,\mathrm{GeV}$ we get

$$G_{\gamma\gamma} = \frac{\Gamma_{\gamma\gamma}(a_f, a_V)}{\Gamma_{\gamma\gamma}(a_f = 1, a_V = 1)} \approx 0.024\,(1.83 a_f - 8.32 a_V)^2 . \tag{2.28}$$

Using the SM values given in tables 2.1 and 2.2 we calculate the signal strength values $\mu_{exp}(a_f, a_V)$ corresponding to the Lagrangian (2.16) as a function of the parameters a_f and a_V . We use the method of least squares described in the appendix A to find the best fit values for the parameters a_f and a_V . That is, we minimize

$$\chi^2(a_f, a_V) = \sum \frac{\left(\mu_{\mathrm{exp}}(a_f, a_V) - \mu_{\mathrm{obs}}\right)^2}{\left(\delta\mu_{\mathrm{obs}}\right)^2} \tag{2.29}$$

with respect to a_f and a_V . From the SM we may expect that the best fit values for a_f and a_V are close to one. Then calculating $\chi_n^2 = \chi_{\mathrm{min}}^2 + \delta_n$ for $\delta_1 = 2.3$, $\delta_2 = 6.18$ and $\delta_3 = 11.83$ we obtain the $1\sigma = 68\%$, $2\sigma = 95\%$ and $3\sigma = 99.7\%$ contours in the (a_f, a_V) -plane. Figure 2.3 shows the best fit point together with the 1σ , 2σ and 3σ confidence level (CL) regions. The best fit point $(a_f, a_V) = (0.96, 1.04)$ is very close to the SM prediction $(a_f, a_V) = (1, 1)$.

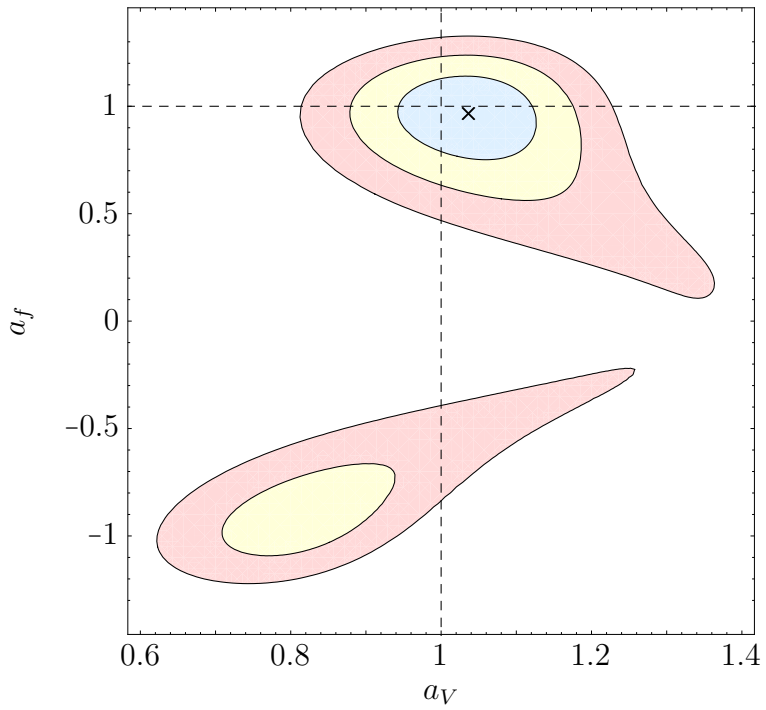

Figure 2.3. Two parameter a_f, a_V fit. Blue, yellow and red areas correspond 1σ, 2σ and 3σ CL regions and cross corresponds to the best fit point. The SM corresponds the intersection of the dotted lines.

Chapter 3

Need to go beyond

Despite the success of the SM it is clear that it can not be the fundamental theory of elementary particle interactions. There are phenomenological and conceptual problems with the SM, of which we will next briefly explain the hierarchy problem, the dark matter problem and the baryon asymmetry problem. For more complete reviews on dark matter see references [27, 28] , and on baryon asymmetry see e.g. [29] . The hierarchy problem is considered for example in the references [30, 31] .

3.1 Hierarchy problem

It is clear that one needs spontaneous breaking of $\mathrm{SU(2)_L} \times \mathrm{U(1)_Y}$ at the energy scale $\sim 100\,\mathrm{GeV}$. Less clear is how the symmetry breaking happens. In the SM one introduces fundamental scalar fields to break the symmetry. This leads to the hierarchy problem. If we consider radiative corrections to the Higgs boson mass arising from its self-interactions and couplings with gauge boson and fermions, we find a quadratic divergence of the Higgs mass. This leads to unnatural fine-tuning in order to obtain the observed mass and to not break SM already at the few TeV scale.

There are at least three fundamental energy scales in nature: electroweak scale, described in the SM by $v_{\mathrm{weak}} = 246\,\mathrm{GeV}$, QCD scale $\Lambda_{\mathrm{QCD}} \sim 0.1\,\mathrm{GeV}$, where the perturbative QCD coupling constant diverges, and Planck scale $M_{\mathrm{Planck}} \sim 10^{19}\,\mathrm{GeV}$, where gravity becomes as strong as the gauge interactions. The smallness of the QCD scale compared to the Planck scale is understood: Starting from the Planck scale, the running of the QCD coupling,

$$\alpha(\Lambda) = \frac{\alpha(M^2_{\mathrm{Planck}})}{1 + \beta_0 \alpha(M^2_{\mathrm{Planck}}) \ln\left(\frac{\Lambda^2}{M^2_{\mathrm{Planck}}}\right)} \,, \tag{3.1}$$

naturally gives $\Lambda_{\mathrm{QCD}} \ll M_{\mathrm{Planck}}$, since from the equation (3.1) we get

$$\ln\left(\frac{\Lambda_{\mathrm{QCD}}}{M_{\mathrm{Planck}}}\right) = \frac{1}{2\beta_0}\left(\frac{1}{\alpha(\Lambda_{\mathrm{QCD}})} - \frac{1}{\alpha(M_{\mathrm{Planck}})}\right) = -\frac{1}{2\beta_0\alpha(M_{\mathrm{Planck}})} , \quad (3.2)$$

which for $\alpha(M_{\mathrm{Planck}}) \sim 0.01$ and $\beta_0 \sim 1$ gives $\Lambda_{\mathrm{QCD}}/M_{\mathrm{Planck}} \sim 10^{-20}$. The electroweak scale, in turn, is not understood within the SM.

Perhaps the fundamental Higgs boson should be replaced by some composite particle. Technicolor theories [32, 30] provide a dynamical way of breaking the electroweak symmetry. Similarly as in the QCD it would be nice if one could generate the electroweak symmetry breaking scale $\sim 100\,\mathrm{GeV}$ in a natural way. This will lead to composite Higgsses. However, these composite particles can be in effective models described by scalar fields. Hence the models we study in this thesis may as well describe composite particles as fundamental scalar particles.

There are also other theoretical problems in the SM. One may ask why there are just three generations of fermions. Or how to explain the huge hierarchy of the fermion masses. The SM does not give answers to these questions.

3.2 Dark matter

There are plenty of astrophysical evidences for dark matter. The first signs of dark matter emerged in the 1930s as Fritz Zwicky studied the movement of galaxies within the Coma Cluster [33] . He determined the velocities of the galaxies by measuring their Doppler shifts. According to the virial theorem

$$2\overline{E_{\mathrm{kin}}} = -\overline{E_{\mathrm{pot}}} , \quad (3.3)$$

where $\overline{E_{\mathrm{kin}}}$ is the average total kinetic energy and $\overline{E_{\mathrm{pot}}}$ the average total potential energy of particles interacting with each other through gravitational force. Now

$$\overline{E_{\mathrm{kin}}} = \frac{1}{2}M_{\mathrm{tot}}\overline{v^2} , \quad (3.4)$$

where M_{tot} is the total mass of the cluster and $\overline{v^2}$ is the average squared velocity of the individual nebulae. Assuming that the nebulae are uniformly distributed inside a sphere of radius R the average total potential energy of the cluster is

$$\overline{E_{\mathrm{pot}}} = \frac{-3GM_{\mathrm{tot}}^2}{5R} . \quad (3.5)$$

Thus the from the virial theorem (3.3) we get

$$M_{\text{tot}} = \frac{5R\overline{v^2}}{3G} \ . \tag{3.6}$$

But the assumption of uniform distribution is actually not fulfilled. Looking at the distribution of the brightest nebulae in the Coma Cluster Zwicky ended up with the following approximation for the total mass of the cluster:

$$M_{\text{tot}} > \frac{R\overline{v^2}}{5G} \ . \tag{3.7}$$

He found that the average mass of one galaxy in the Coma Cluster is $M = 4.5 \cdot 10^{10} M_\odot$ whereas the luminosity of an average galaxy is $L = 8.5 \cdot 10^7 L_\odot$. Hence he concluded that there must be some non-luminous matter which accounts for most of the total mass of the Coma Cluster.

Later in the 1970s similar phenomena was observed also in galaxies. It was observed that the galactic rotation curves are not in agreement with the theoretical calculations which take into account only the luminous matter. Assuming that the total mass M of the galaxy is centrally concentrated it follows, according to Newtonian gravity, that the velocity distribution far from the center of the galaxy is

$$v(r) = \sqrt{\frac{MG}{r}} \propto \frac{1}{\sqrt{r}} \ . \tag{3.8}$$

However, as shown in figure 3.1, the measured velocity distribution turns out to be constant at large distances. Hence the mass distribution of the galaxy is $M(r) \propto r$, so

$$4\pi r^2 \rho(r) = \text{const.} \implies \rho(r) \propto \frac{1}{r^2} \ . \tag{3.9}$$

This density distribution is just the distribution given by a non-interacting isothermal gas. The pressure of the gas must be in equilibrium with gravitation, so

$$\frac{\mathrm{d}p}{\mathrm{d}r} = -\frac{GM(r)\rho(r)}{r^2} \ , \tag{3.10}$$

where $M(r) = \int_0^r \rho(r)\mathrm{d}r$. Now the pressure of the gas can be calculated using the ideal gas law

$$p(r) = \rho(r)\frac{k_B T}{m} \ , \tag{3.11}$$

where the temperature T is constant and m is the mass of an individual gas particle. Combining equations (3.10) and (3.11) we obtain

$$\frac{k_B T}{4\pi G m}\frac{\mathrm{d}}{\mathrm{d}r}\left(\frac{r^2}{\rho}\frac{\mathrm{d}\rho}{\mathrm{d}r}\right) = -r^2\rho \ . \tag{3.12}$$

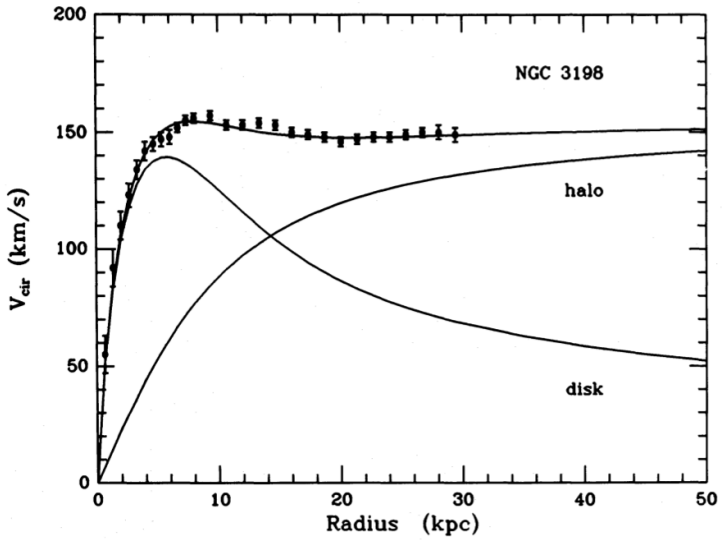

Figure 3.1. Rotation curve of the spiral galaxy NGC 3198 [34].

So the density distribution of a non-interacting isothermal gas is $\rho \propto r^{-2}$.

The observation of missing matter in the galaxy clusters and galaxies could be explained by a halo consisting of non-interacting particles, but also by modified Newtonian dynamics [35] . However, there is more convincing evidences for the dark matter, most importantly from the observations of the Bullet Cluster [36] . The Bullet Cluster consists of two colliding galaxy clusters. In the collision of two galaxy clusters stars (visible component) are not greatly affected but the hot intra-cluster baryonic gas (X-ray component) is slowed down and left behind. The mass of the baryonic gas is much larger than the total mass of the stars, thus the gravitational lensing would be expected to be strongest from the collision center. Composite image 3.2 of the Bullet Cluster shows the locations of the baryonic gas detected by Chandra X-ray Observatory and the regions where the observed gravitational lensing is strongest. Observations show that the lensing is strongest near the visible galaxies, which favors the idea of collisionless dark matter halo. Furthermore structure formation and results from the WMAP [37] and Planck [8] satellites support the existence of dark matter.

There are several dark matter candidates including massive compact halo objects (MACHOs), axions and weakly interacting massive particles (WIMPs). Analysis of structure formation indicates that dark matter should be cold (i.e. non-relativistic). Dark matter candidate particles should interact very weakly with photons because otherwise it would not be non-luminous. Moreover the dark matter candidate should be stable (or very long-lived), so it would not have decayed by now. We will now concentrate on WIMPs, which provide the

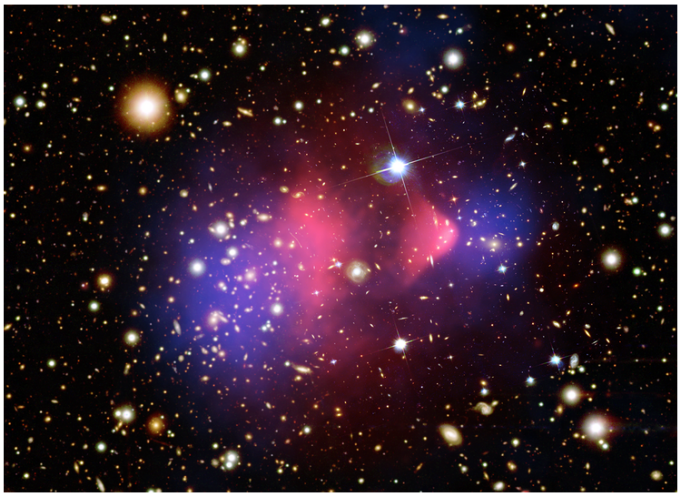

Figure 3.2. Composite image of the Bullet Cluster 1E 0657-56. Red areas correspond to the baryonic gas detected by Chandra X-ray Observatory and blue areas show where the most of the mass of the clusters is located.

most favorable candidates for the dark matter.

According to the WIMP-scenario dark matter consists of new elementary particles with masses roughly between 10 GeV and a few TeV , and with annihilation cross-section of approximatively weak strength. In the early Universe, WIMPs were in thermal equilibrium with visible matter. Due to the rapid expansion of the Universe, the mean free path of the WIMPs grew larger than the size of the Universe and dark matter froze out of the equilibrium. It can be shown that the relic density of WIMPs today is

$$\Omega \propto \frac{1}{\langle v\sigma \rangle} \sim \frac{m^2}{g^4} \,, \tag{3.13}$$

where $\langle v\sigma \rangle$ is the thermally-averaged annihilation cross-section of the WIMPs, m is the mass of the WIMP and g is the coupling constant characterizing the annihilation. If the mass of the WIMPs is $m \sim 100\,\mathrm{GeV}$ and the coupling is weak $g \sim g_{\mathrm{weak}} \approx 0.65$ then $\Omega \sim 0.23$. Remarkably this is very close to the measured value $\Omega_{\mathrm{obs}} = 0.26$ [8] . This is often called the WIMP miracle: WIMPs naturally produce the observed dark matter relic density. The SM does not provide a WIMP candidate, but in its extensions various WIMP candidates have been proposed including lightest supersymmetric particle, sterile neutrinos and different new scalar particles.

Dark matter sector may consist of only a single new particle, but it could also be larger. In principle there is no evident reason why there would not

exist a new sector manifesting some gauge symmetry and consisting of fields that transform as singlets under the SM gauge group. Fields that are singlets under SM gauge group can not couple to SM gauge bosons nor SM fermions, but they can couple to Higgs boson. Hence the Higgs boson provides a portal between the SM and the hidden sector. These so-called Higgs portal models have been studied for example in the references [38, 39] . The coupling of Higgs boson with the hidden sector may modify the couplings of Higgs with the SM particles and may provide an invisible decay channel of the Higgs boson. These can be constrained using the Higgs coupling data available from the LHC and Tevatron experiments.

WIMPs interact only through gravitational and weak interactions so they are very difficult to detect. There are, however, many experiments attempting to observe WIMPs directly. Direct measurement of WIMPs is based on elastic scattering of WIMPs on nuclei. One can try to look for the annual modulation of scattering events due to Earth's rotation around the Sun or one may reduce the background events (mostly due to cosmic rays) near zero and measure just the WIMP-nucleon scattering.

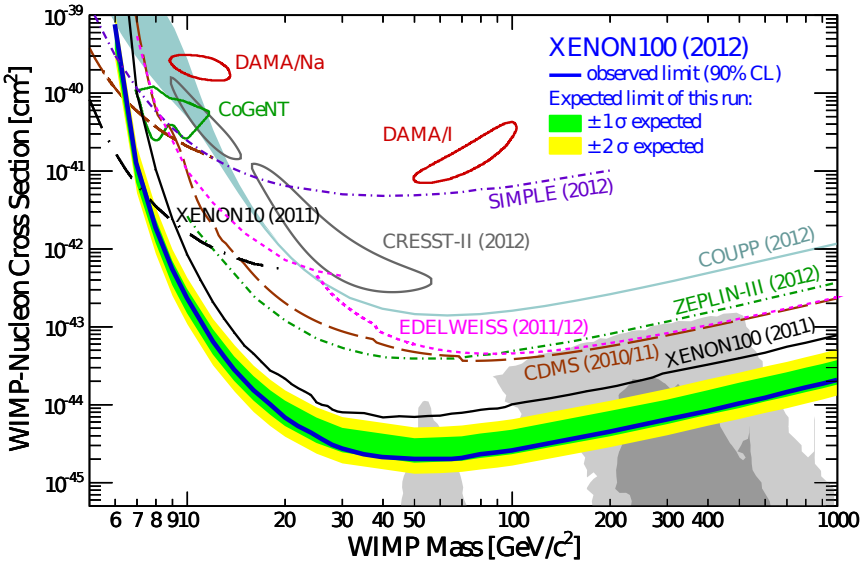

Figure 3.3. Spin-independent upper limits for the WIMP-nucleon cross-section as a function of WIMP mass from various different experiments. Also the DAMA, CoGent and CRESST-II favored WIMP signal regions are shown [40].

WIMPs have not been directly observed yet. This gives upper limits for the WIMP-nucleon cross-section. The scattering of the WIMP off of nuclei is generally divided in two classes: spin-dependent and spin-independent scattering. For spin-independent scattering the cross-section is approximatively

proportional to the WIMP-proton cross-section, $\sigma \propto A^2\sigma_p$, where A is the mass number of the nucleus. In the spin-dependent case the cross-section depends on the nuclear spin rather than the mass number. Current direct searches use heavy target nuclei, so the spin-independent cross-section is dominating over the spin-dependent cross-section and the direct searches give upper limits on the spin-independent cross-section. In figure 3.3 upper limits for the spin-independent cross-section arising from the direct searches are shown.

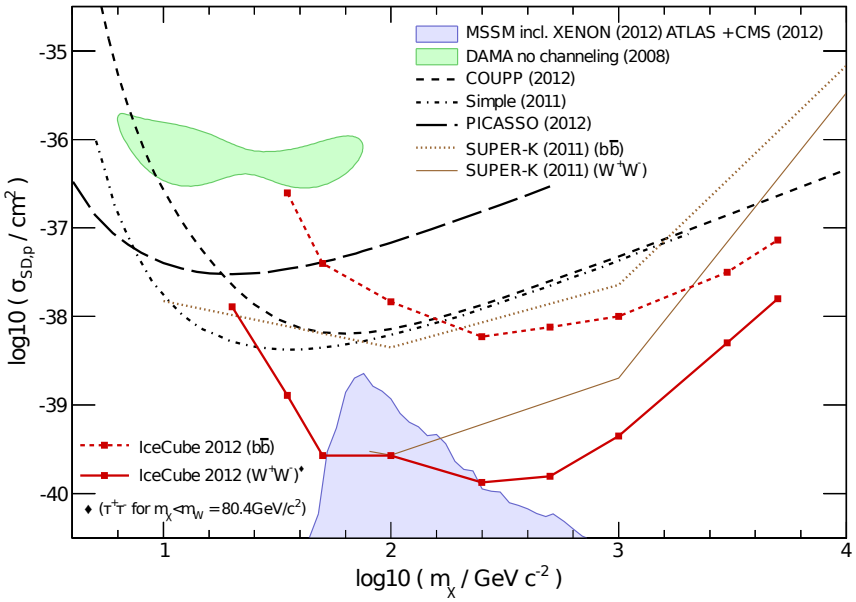

Figure 3.4. Spin-dependent upper limits for the WIMP-nucleon cross-section as a function of WIMP mass from various different experiments [41].

There are also experiments attempting to observe WIMPs indirectly. Indirect searches based on the annihilation of WIMPs are trying to observe the annihilation products. Celestial objects like the Sun and the Earth can slow down WIMPs and capture them, so the annihilation probability in the core of the Sun can be larger than in the surrounding space. The annihilation products may include for example neutrinos. Large neutrino telescopes including Super-Kamiokande and IceCube have tried to measure these neutrinos. However, no significant excess over the expected atmospheric neutrino background is observed yet. Because the Sun is mostly made of light elements, the indirect searches give bounds on the spin-dependent cross-section. These limits are shown in figure 3.4 .

3.3 Baryogenesis

Astrophysical evidences have shown that our galaxy and its neighborhood are predominantly made of matter. Moreover it has been shown that the Universe can not consist of distinct regions of matter and antimatter [42] . Hence there is a clear asymmetry between matter and antimatter. The asymmetry is characterized by baryon-to-photon ratio

$$\eta = \frac{n_b - n_{\bar{b}}}{n_\gamma} \ , \tag{3.14}$$

where n_b and $n_{\bar{b}}$ are the number densities of baryons and antibaryons, respectively, and n_γ is the number density of photons. According to WMAP observations $\eta = 6.19 \cdot 10^{-10}$ [43] . The goal of baryogenesis is to explain why η is not zero as one would a priori expect, assuming that the Universe was out baryon-symmetric after inflation.

There are three ingredients, known as Sakharov conditions [44] , which should be fulfilled in order to produce the baryon asymmetry:

1. baryon number violation,
2. C and CP violation,
3. departure from thermal equilibrium.

The first ingredient is trivial: There has to be at least one process which does not conserve the baryon number (= number of baryons − number of antibaryons), otherwise the baryon number would be zero forever. However, the existence of baryon number violating process is not enough to produce baryon asymmetry, since the baryon number is odd under C and CP , and if the C and CP symmetries are satisfied the baryon number violating process would have the same cross-section as its C- and CP-conjugate processes. Thus C and CP symmetries must be violated. The third condition is clear because initially the number densities of baryons and antibaryons were the same and the mass of particle is the same as the mass of the corresponding antiparticle, so in the thermal equilibrium the number densities evolve similarly. Hence the number densities would be the same forever if there would not be a departure from thermal equilibrium.

There are many different mechanisms for baryogenesis [45–49] , most popular of which are electroweak baryogenesis (EWBG), leptogenesis and GUT baryogenesis. In particular EWBG is very attractive both theoretically and experimentally. In the EWBG the baryogenesis occurs during the electroweak phase transition, thus the energy scale of the processes is $\sim 100\,\mathrm{GeV}$. According to EWBG during the electroweak phase transition the baryon number

violating processes took place at the interphase and due to C and CP violation the baryon generating processes were dominating over the antibaryon generating processes.

The SM fulfills the Sakharov conditions, but the SM mechanisms do not produce large enough baryon-to-photon ratio. This is so because the only source of CP violation in the SM is the Kobayashi-Maskawa phase [50] , which has been claimed to be too weak for the observed baryon-to-photon ratio [51] . Moreover, the departure from thermal equilibrium in the SM occurs during the electroweak phase transition, that is not a strong first order phase transition [52] as required for successful electroweak baryogenesis. Hence, for the baryogenesis the SM should be extended such that it includes new sources of CP violation and modifies the electroweak phase transition or introduces new sources for departure from thermal equilibrium.

Chapter 4

Standard Model with one real singlet Higgs

Maybe the simplest way to extend the SM Higgs sector is to consider in addition to one doublet scalar ϕ also a real singlet scalar S . The main motivation to study the singlet extension of the SM is the dark matter problem. The singlet S could provide a good dark matter candidate. The first detailed analysis of the singlet scalar dark matter model was presented by John McDonald [53] and more recently it has been studied for example in the references [54, 55] .

The scalar potential of the singlet extension is

$$V(\phi, S) = V(\phi) - \mu_S^2 S^2 + \frac{\lambda_S}{4} S^4 + \frac{\lambda_m}{2} S^2 \phi^\dagger \phi \,, \tag{4.1}$$

where $V(\phi)$ is the SM scalar potential (2.4) . In principle we could add terms S^3 and $S\phi^\dagger\phi$ to the potential, but we require stability of S , since we will consider S as a dark matter particle, so it should not decay. Hence the potential has Z_2 symmetry $S \to -S$.

The doublet ϕ acquires VEV as in the SM. To be general we first allow also the singlet S to have a non-zero VEV $\langle S \rangle = \omega \neq 0$. This will break the Z_2 symmetry, but we will see that the LHC data actually forces $\omega = 0$. From the conditions

$$\left.\frac{\partial V}{\partial \phi_r}\right|_{\text{vacuum}} = \left.\frac{\partial V}{\partial S}\right|_{\text{vacuum}} = 0 \tag{4.2}$$

we get

$$\mu^2 = \frac{1}{4}\left(\lambda v^2 + \lambda_m \omega^2\right) \;,\;\; \mu_S^2 = \frac{1}{4}\left(\lambda_m v^2 + \lambda_S \omega^2\right) \;. \tag{4.3}$$

As in the SM there is no mixing between the real and imaginary parts of the neutral component of the doublet

$$\phi = \begin{pmatrix} \phi^+ \\ \phi_r + \mathrm{i}\phi_i \end{pmatrix} \,, \tag{4.4}$$

and the imaginary component of the neutral part becomes the neutral Goldstone boson and the charged part becomes the charged Goldstone boson. These give the longitudinal polarization degrees to the Z and W bosons. The mass matrix for the neutral real scalar fields in the basis $\{\phi_r, S\}$ is

$$M^2 = \frac{1}{2}\begin{pmatrix} \lambda v^2 & \lambda_m v\omega \\ \lambda_m v\omega & \lambda_S \omega^2 \end{pmatrix} . \tag{4.5}$$

A general real symmetric 2×2 matrix

$$\begin{pmatrix} A & B \\ B & C \end{pmatrix} \tag{4.6}$$

can be diagonalized by a rotation

$$R_2 = \begin{pmatrix} \cos\theta & \sin\theta \\ -\sin\theta & \cos\theta \end{pmatrix} , \tag{4.7}$$

through an angle θ defined by

$$\tan(2\theta) = \frac{2B}{A-C} . \tag{4.8}$$

Hence, with the rotation by angle β which satisfies

$$\tan(2\beta) = \frac{2\lambda_m v\omega}{\lambda v^2 - \lambda_S \omega^2} \tag{4.9}$$

we get to the mass eigenbasis where the mass matrix (4.5) is diagonal. The mass eigenstates are

$$h = \phi_r \cos\beta - S\sin\beta , \quad S_0 = \phi_r \sin\beta + S\cos\beta . \tag{4.10}$$

The singlet S does not couple to gauge bosons and fermions, whereas the doublet ϕ couples with them as in the SM. Let us assume that h corresponds to the observed Higgs boson. Now $\phi_r = h\cos\beta + S_0 \sin\beta$, thus the couplings of h to the gauge bosons and fermions are given by the SM couplings multiplied with the factor $\cos\beta$. Writing $a_V = a_f := a$ we may use the analysis introduced in section 2.3 to fit the angle β to the Higgs decay data. Minimizing χ^2 gives the best fit $a = 1.02$ so that the data prefers the angle $\beta = 0$, that gives the SM couplings. In figure 4.1 the 1σ , 2σ and 3σ regions are shown.

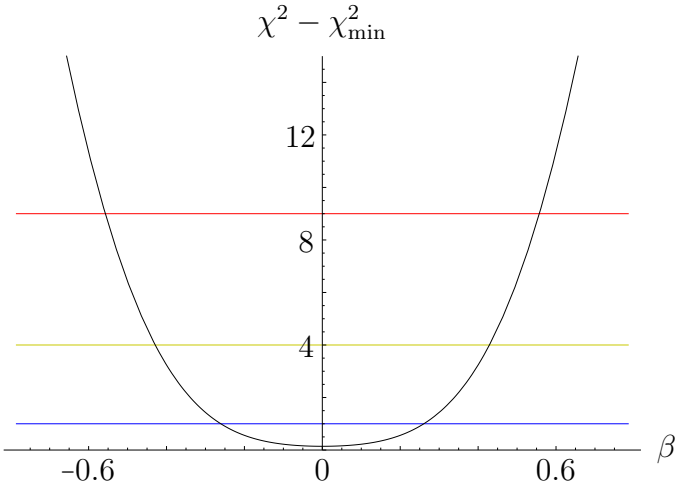

Figure 4.1. One parameter β fit. Blue, yellow and red lines correspond 1σ, 2σ and 3σ CL regions. The angle β is measured in radians.

4.1 Invisible decay of Higgs boson

The angle $\beta = 0$ corresponds to the case where the VEV of the singlet is zero, $\omega = 0$, which is also required for S to be dark matter. In the $\omega = 0$ case the mass matrix of the neutral real fields is diagonal

$$M^2 = \frac{1}{2}\begin{pmatrix} \lambda v^2 & 0 \\ 0 & \lambda_m v^2 - 4\mu_S^2 \end{pmatrix} \tag{4.11}$$

and $h = \phi_r$ is the Higgs boson with mass $m_h^2 = \lambda v^2/2$. Now $a_f = 1 = a_V$, but if we assume that the mass of the singlet S ,

$$m_S^2 = \frac{\lambda_m v^2}{2} - 2\mu_S^2 \, , \tag{4.12}$$

is less than half of the Higgs mass there is a Higgs decay channel $h \to SS$. This decay channel would be invisible for the experiments, because S does not interact with the SM gauge bosons and fermions. The invisible decay channel affects only to the total decay width $\Gamma_{\rm tot}$. We may write

$$\frac{\Gamma_{\rm tot}}{\Gamma_{\rm SMtot}} = \sum_k G_k {\rm BR}_k + \frac{\Gamma_{\rm inv}}{\Gamma_{\rm SMtot}} \, , \tag{4.13}$$

where the sum includes the SM Higgs decay channels. Now $G_k = 1$ for all SM Higgs decay channels and $s_k = 1$ for all production channels so

$$\frac{\Gamma_{\rm tot}}{\Gamma_{\rm SMtot}} = 1 + \frac{\Gamma_{\rm inv}}{\Gamma_{\rm SMtot}} \, , \tag{4.14}$$

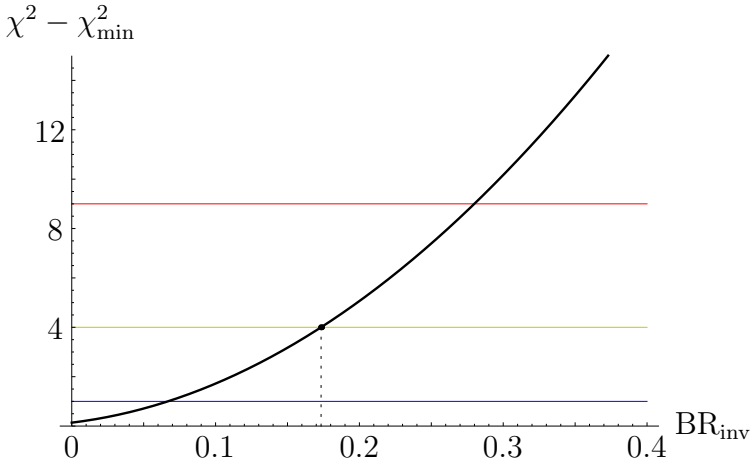

Figure 4.2. One parameter $\rm BR_{inv}$ fit. Blue, yellow and red lines correspond 1σ, 2σ and 3σ CL regions. The dashed line at $BR_{\rm inv} = 0.17$ shows the 2σ value.

and

$$\mu_j = \frac{\Gamma_{\rm SMtot}}{\Gamma_{\rm inv} + \Gamma_{\rm SMtot}} = 1 + \rm BR_{inv} \ , \tag{4.15}$$

where $\rm BR_{inv} = \Gamma_{inv}/(\Gamma_{inv} + \Gamma_{SMtot})$. Minimizing χ^2 gives $\rm BR_{inv} = -0.04$ thus the data prefers no invisible decay channel. Figure 4.2 shows the 1σ , 2σ and 3σ regions. The 2σ limit for the branching ratio to the invisible decay channel is

$$\rm BR_{inv}(2\sigma) = 0.17 \ . \tag{4.16}$$

We may also calculate the branching ratio for the invisible Higgs decay channel from the model as a function of the singlet mass m_S and the parameter λ_m . Now

$$\Gamma_{\rm inv} = \frac{|M_{h\to SS}|^2}{16\pi m_h}\sqrt{1 - \frac{4m_S^2}{m_h^2}} \ , \tag{4.17}$$

and to the lowest order the amplitude is trivial,

$$M_{h\to SS} = \frac{\lambda_m v}{2} \ , \tag{4.18}$$

thus

$$\Gamma_{\rm inv} = \frac{\lambda_m^2 v^2}{32\pi m_h}\sqrt{1 - \frac{4m_S^2}{m_h^2}} \ . \tag{4.19}$$

In figure 4.3 the 1σ , 2σ and 3σ contours in the (λ_m, m_S) -plane are shown. We can write the 2σ limit (4.16) as a constraint on the λ_m parameter if $2m_S < m_h$:

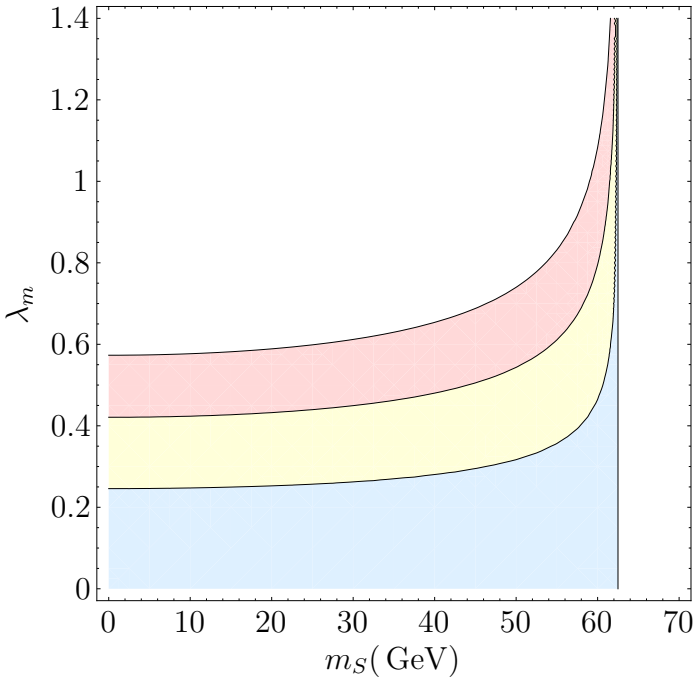

Figure 4.3. 1σ (blue), 2σ (yellow) and 3σ (red) CL regions in the (λ_m, m_S) -plane corresponding to the constraints arising from the $h \to SS$ decay.

$$\lambda_m < 4.65 \left(\frac{\text{GeV}}{m_h^2 - 4m_S^2} \right)^{1/4} . \tag{4.20}$$

4.2 Dark matter relic abundance

An interesting quantity, which we can calculate from the singlet extension of the SM, is the relic abundance of the dark matter candidate. It tells us how much of the total amount of the dark matter could be formed by the singlet scalar candidate. Decoupling of dark matter particles (WIMPs) from the visible matter is described by the Lee-Weinberg equation [56]

$$\frac{\mathrm{d}n}{\mathrm{d}t} = -3Hn + \langle v\sigma \rangle \left(n_{\text{eq}}^2 - n^2 \right) , \tag{4.21}$$

where n is the particle number density of the WIMPs, n_{eq} is the particle number density in the thermal equilibrium, $\langle v\sigma \rangle$ is the flux-weighted thermally averaged annihilation cross-section of the WIMPs and $3Hn$ describes the reduction of the annihilation rate due to the expansion of the Universe. From the Lee-Weinberg equation we can solve the relic abundance Ωh^2 of the WIMPs.

An approximative solution is given in the appendix B. The solution is

$$\Omega h^2 = -5.196 \cdot 10^8 \,\mathrm{GeV}^{-1} \, \frac{m_S}{x_f Z(x_f)} \; . \tag{4.22}$$

where

$$Z(x) = -\sqrt{\frac{\pi}{45} g_* \left(\frac{m_S}{x}\right)} M_{\mathrm{Planck}} m_S x^{-2} \langle v\sigma \rangle (x) \; . \tag{4.23}$$

The parameter x_f can be iteratively solved from the equation

$$x_f = \ln \left(\frac{Z(x_f) y_{\mathrm{eq}}(x_f)^2}{\left. \frac{\mathrm{d}y_{\mathrm{eq}}}{\mathrm{d}x} \right|_{x_f} - y_{\mathrm{eq}}(x_f)} \right) \; , \tag{4.24}$$

where

$$y_{\mathrm{eq}}(x) = \frac{45}{4\pi^4 g_*(\frac{m_S}{x})} x^2 \mathrm{e}^x K_2(x) \; . \tag{4.25}$$

Functions K_n are the modified Bessel functions of second kind. According to the latest Planck data [8] the dark matter relic abundance is $\Omega_{\mathrm{obs}} h^2 \approx 0.1199 \pm 0.0027$.

We only need to calculate the flux-weighted annihilation cross-section from the model. There are three different types of annihilation channels: Higgs channel $SS \to hh$, vector boson channel $SS \to VV$ and fermion channel $SS \to f\overline{f}$. In the appendix C we have calculated these annihilation cross-sections in a more general case. Now the interactions are described by the Lagrangians

$$\mathcal{L}_{\mathrm{scalar}} = \frac{\lambda_m v}{4} h S^2 + \frac{\lambda v}{4} h^3 + \frac{\lambda_m}{8} h^2 S^2 \tag{4.26}$$

$$\mathcal{L}_{\mathrm{gauge}} = \frac{2M_W^2}{v} g^{\mu\nu} h W_\mu^+ W_\nu^- + \frac{M_Z^2}{v} g^{\mu\nu} h Z_\mu Z_\nu \tag{4.27}$$

and

$$\mathcal{L}_{\mathrm{fermion}} = \frac{m_f^2}{\sqrt{2}v} h \psi_f \overline{\psi}_f \; . \tag{4.28}$$

Inserting the above couplings in the formulae given in the appendix C we get

$$\begin{aligned}
\sigma_{hh} &= \frac{v_h}{64\pi s v_S} \left(\lambda_m + \frac{3\lambda_m m_h^2}{s - m_h^2} - \frac{\lambda_m^2 v^2}{s - 2m_h^2} \right)^2 \; , \\
\sigma_{VV} &= \frac{v_V}{8\pi s v_S} \frac{\lambda_m^2 M_V^4}{\left(s - m_h^2\right)^2} \left(3 + \frac{s(s - 4M_V^2)}{4M_V^4} \right) \cdot \begin{cases} 1 & , \, W \\ \frac{1}{8} & , \, Z \end{cases} \; , \\
\sigma_{ff} &= \frac{v_f N_c}{512\pi s v_S} \frac{\lambda_m^2 m_f^2 \left(s - 4m_f^4\right)}{\left(s - m_h^2\right)^2} \; ,
\end{aligned} \tag{4.29}$$

where

$$v_X = \sqrt{1 - \frac{4m_X^2}{s}} \ . \tag{4.30}$$

The flux-weighted thermally averaged annihilation cross-section can be calculated using the formula

$$\langle v\sigma \rangle(x) = \frac{x}{8m_S^5 K_2^2(x)} \int_{4m_S^2}^{\infty} \mathrm{d}s \sqrt{s}(s - 4m_S^2) K_1 \left(\frac{\sqrt{s}}{m_S} x \right) \sigma_{tot}(s) \ , \tag{4.31}$$

where

$$\sigma_{tot} = \sigma_h + \sigma_Z + \sigma_W + \sum \sigma_f \ . \tag{4.32}$$

The relic abundance divided by the observed value $\Omega_{\mathrm{obs}} h^2 \approx 0.12$ for four different λ_m is shown in figure 4.4 .

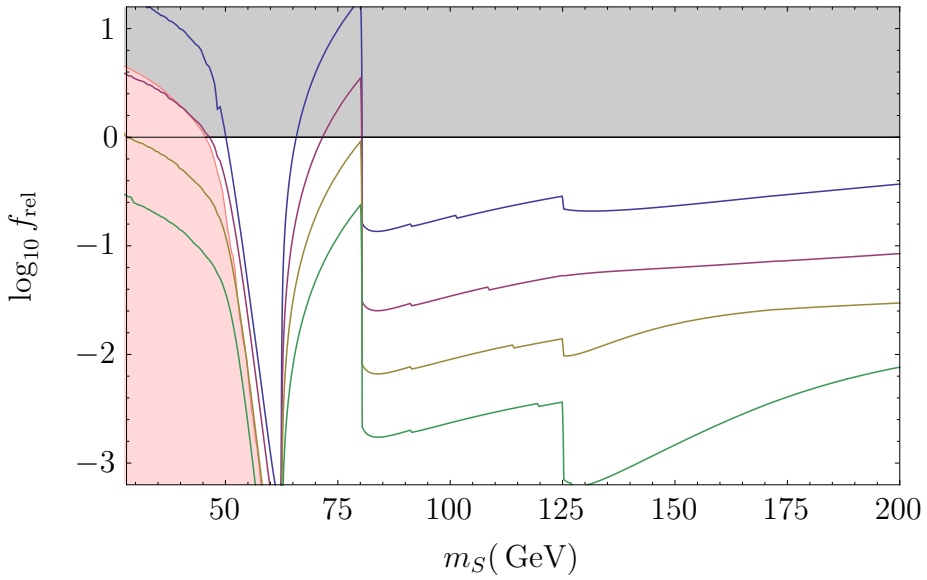

Figure 4.4. Logarithm of $f_{\mathrm{rel}} = \Omega h^2 / 0.12$ as a function of the singlet mass m_S . The curves from top to down correspond λ_m values 0.2, 0.5, 1.0 and 2.0, respectively. Red region is excluded by the 2σ limit for the $h \to SS$ decay branching ratio and the gray region is excluded by the Planck data.

Chapter 5

Two-Higgs-doublet model with one real singlet Higgs

5.1 Two-Higgs-doublet model

The two-Higgs-doublet model (2HDM) includes two scalar doublets with identical quantum numbers

$$\phi_1 = \begin{pmatrix} \phi_1^+ \\ \phi_1^0 \end{pmatrix} , \quad \phi_2 = \begin{pmatrix} \phi_2^+ \\ \phi_2^0 \end{pmatrix} \tag{5.1}$$

giving eight real degrees of freedom. Three degrees of freedom are eaten by the W and Z bosons and the remaining degrees of freedom are realized as five massive scalar bosons. The scalar sector of the 2HDM is

$$\mathcal{L}_{\text{Higgs}} = (D_\mu \phi_1)^\dagger (D^\mu \phi_1) + (D_\mu \phi_2)^\dagger (D^\mu \phi_2) - V(\phi_1, \phi_2) , \tag{5.2}$$

where the scalar potential $V(\phi_1, \phi_2)$ is a combination of gauge invariant terms $\phi_i^\dagger \phi_j$, $i, j = 1, 2$. The scalar potential can be written as [57]

$$\begin{aligned} V(\phi_1, \phi_2) = {} & \mu_1^2 \phi_1^\dagger \phi_1 + \mu_2^2 \phi_2^\dagger \phi_2 - \mu_{12}^2 \phi_1^\dagger \phi_2 - (\mu_{12}^2)^* \phi_2^\dagger \phi_1 \\ & + \frac{\lambda_1}{2} \left(\phi_1^\dagger \phi_1 \right)^2 + \frac{\lambda_2}{2} \left(\phi_2^\dagger \phi_2 \right)^2 + \lambda_3 \phi_1^\dagger \phi_1 \phi_2^\dagger \phi_2 + \lambda_4 \phi_1^\dagger \phi_2 \phi_2^\dagger \phi_1 \\ & + \frac{\lambda_5}{2} \left(\phi_1^\dagger \phi_2 \right)^2 + \frac{\lambda_5^*}{2} \left(\phi_2^\dagger \phi_1 \right)^2 \\ & - \phi_1^\dagger \phi_1 \left(\lambda_6 \phi_1^\dagger \phi_2 + \lambda_6^* \phi_2^\dagger \phi_1 \right) - \phi_2^\dagger \phi_2 \left(\lambda_7 \phi_1^\dagger \phi_2 + \lambda_7^* \phi_2^\dagger \phi_1 \right) , \end{aligned} \tag{5.3}$$

where parameters $\mu_1^2, \mu_2^2, \lambda_1, \lambda_2, \lambda_3, \lambda_4$ are real due to hermiticity of the Lagrangian and parameters $\mu_{12}^2, \lambda_5, \lambda_6, \lambda_7$ are in general complex. Hence the

potential includes 14 real parameters. We begin with the CP conserving case where also the parameters $\mu_{12}^2, \lambda_5, \lambda_6, \lambda_7$ are real, so the number of real parameters reduces to 10. In section 5.2 we will consider the case with most general complex parameters.

The vacuum of the model is characterized by VEVs

$$\langle\phi_1\rangle = \begin{pmatrix} 0 \\ \frac{v_1}{\sqrt{2}} \end{pmatrix} \ , \quad \langle\phi_2\rangle = \begin{pmatrix} 0 \\ \frac{v_2}{\sqrt{2}} \end{pmatrix} \ . \tag{5.4}$$

From the kinetic terms $(D_\mu\phi_1)^\dagger (D^\mu\phi_1)$ and $(D_\mu\phi_2)^\dagger (D^\mu\phi_2)$ we obtain the W boson mass $M_W = g^2(v_1^2 + v_2^2)/8$, so $v_1^2 + v_2^2 = v^2$. Hence we write

$$v_1 = v\cos\beta \ , \quad v_2 = v\sin\beta \ , \tag{5.5}$$

where $\beta \in [0, 2\pi[$. From the minimum condition[1] $\partial_{\phi_{1r}} V = 0 = \partial_{\phi_{2r}} V$ we solve parameters μ_1^2 and μ_2^2 . We get

$$\begin{aligned} \mu_1^2 &= -\frac{v_1^3\lambda_1 + v_2\left(-2\mu_{12}^2 + v_1 v_2\lambda_{345} + 3v_1^2\lambda_6 + v_2^2\lambda_7\right)}{2v_1} \ , \\ \mu_2^2 &= -\frac{v_2^3\lambda_2 + v_1\left(-2\mu_{12}^2 + v_1 v_2\lambda_{345} + v_1^2\lambda_6 + 3v_2^2\lambda_7\right)}{2v_2} \ . \end{aligned} \tag{5.6}$$

where $\lambda_{345} = \lambda_3 + \lambda_4 + \lambda_5$.

Now, since all parameters λ_j, μ_k are real, the real and imaginary parts of the neutral scalar fields, which are the CP even sector and CP odd sector, respectively, are decoupled, whereby the potential (5.3) is CP invariant. The mass matrices of the neutral fields are

$$\begin{pmatrix} \frac{2v_1^3\lambda_1 + v_2\left(2\mu_{12}^2 + 3v_1^2\lambda_6\right) - v_2^3\lambda_7}{2v_1} & -\mu_{12}^2 + v_1 v_2\lambda_{345} + \frac{3}{2}v_1^2\lambda_6 + \frac{3}{2}v_2^2\lambda_7 \\ -\mu_{12}^2 + v_1 v_2\lambda_{345} + \frac{3}{2}v_1^2\lambda_6 + \frac{3}{2}v_2^2\lambda_7 & \frac{2v_2^3\lambda_2 - v_1^3\lambda_6 + v_1\left(2\mu_{12}^2 + 3v_2^2\lambda_7\right)}{2v_2} \end{pmatrix} \tag{5.7}$$

for the real parts in the basis $\{\phi_{1r}, \phi_{2r}\}$, and

$$\begin{pmatrix} -\frac{v_2\left(-2\mu_{12}^2 + 2v_1 v_2\lambda_5 + v_1^2\lambda_6 + v_2^2\lambda_7\right)}{2v_1} & \frac{1}{2}\left(-2\mu_{12}^2 + 2v_1 v_2\lambda_5 + v_1^2\lambda_6 + v_2^2\lambda_7\right) \\ \frac{1}{2}\left(-2\mu_{12}^2 + 2v_1 v_2\lambda_5 + v_1^2\lambda_6 + v_2^2\lambda_7\right) & -\frac{v_1\left(-2\mu_{12}^2 + 2v_1 v_2\lambda_5 + v_1^2\lambda_6 + v_2^2\lambda_7\right)}{2v_2} \end{pmatrix} \tag{5.8}$$

for the imaginary parts in the basis $\{\phi_{1i}, \phi_{2i}\}$. For the charged fields the mass matrix in the basis $\{\phi_1^+, \phi_2^+\}$ is

$$\begin{pmatrix} -\frac{v_2\left(-2\mu_{12}^2 + v_1 v_2\lambda_{45} + v_1^2\lambda_6 + v_2^2\lambda_7\right)}{2v_1} & \frac{1}{2}\left(-2\mu_{12}^2 + v_1 v_2\lambda_{45} + v_1^2\lambda_6 + v_2^2\lambda_7\right) \\ \frac{1}{2}\left(-2\mu_{12}^2 + v_1 v_2\lambda_{45} + v_1^2\lambda_6 + v_2^2\lambda_7\right) & -\frac{v_1\left(-2\mu_{12}^2 + v_1 v_2\lambda_{45} + v_1^2\lambda_6 + v_2^2\lambda_7\right)}{2v_2} \end{pmatrix} , \tag{5.9}$$

[1] We denote real and imaginary parts of the neutral scalar fields by ϕ_{kr} and ϕ_{ki} , $k = 1, 2$, respectively.

where $\lambda_{45} = \lambda_4 + \lambda_5$.

We can diagonalize the mass matrix (5.7) by a rotation trough an angle α defined by

$$\tan(2\alpha) = \frac{v_1 v_2 \left(-2\mu_{12}^2 + 2v_1 v_2 \lambda_{345} + 3v_1^2 \lambda_6 + 3v_2^2 \lambda_7\right)}{2\mu_{12}^2(v_2^2 - v_1^2) + 2v_1^3 v_2 \lambda_1 - 2v_1 v_2^3 \lambda_2 + v_1^4 \lambda_6 + 3v_1^2 v_2^2 \left(\lambda_6 - \lambda_7\right) - v_2^4 \lambda_7} , \tag{5.10}$$

and the mass matrices (5.8) and (5.9) we can diagonalize by a rotation trough an angle

$$\beta = \frac{1}{2} \arctan\left(\frac{2v_1 v_2}{v_1^2 - v_2^2}\right) = \arctan \frac{v_2}{v_1} . \tag{5.11}$$

After the symmetry breaking we obtain five massive scalar bosons: two neural CP even scalars h and H , one neutral CP odd scalar A_0 and two charged scalars $H^\pm$. The three $m = 0$ Goldstone bosons are removed from the physical spectrum. The massive mass eigenstates are

$$\begin{pmatrix} h \\ H \end{pmatrix} = \begin{pmatrix} \cos\alpha & -\sin\alpha \\ \sin\alpha & \cos\alpha \end{pmatrix} \begin{pmatrix} \phi_{1r} \\ \phi_{2r} \end{pmatrix} , \tag{5.12}$$

$$A_0 = \phi_{1i} \cos\beta - \phi_{2i} \sin\beta \tag{5.13}$$

and

$$H^\pm = \phi_1^\pm \cos\beta - \phi_2^\pm \sin\beta . \tag{5.14}$$

The Yukawa sector of the 2HDM may be rather complicated. Either (or both) of the doublets can in principle have Yukawa couplings with fermions. In practice there are three different popular scenarios: type I 2HDM where all the fermions couple to just one of the Higgs doublets [58], type II 2HDM where down-type quarks and leptons couple to one of the Higgs doublets and up-type quarks to the other Higgs doublet [59], and type III where both of the Higgs doublets couple to all fermions [60]. In the following we will consider type I 2HDM and choose that the doublet ϕ_2 couples to the fermions. Hence the Yukawa Lagrangian is

$$\mathcal{L}_{\text{Yuk}} = Y_e \overline{\psi}_{l,L}^T \phi_2 \psi_{e,R} + Y_u \overline{\psi}_{q,L}^T (-\mathrm{i}\tau_2 \phi_2) \psi_{u,R} + Y_d \overline{\psi}_{q,L}^T \phi_2 \psi_{d,R} + \text{h.c.} . \tag{5.15}$$

5.2 Two-Higgs-doublet model with one real singlet Higgs

Next we combine the type I 2HDM with the singlet model presented in chapter 4. This model could offer enough CP violation for baryogenesis and the singlet

S could provide a good WIMP candidate. We call this model two-Higgs-doublet-inert-singlet model (2HDISM). We analyze the model constraining it by the electroweak precision data and the Higgs decay data, and calculate the relic abundance of the dark matter candidate as in section 4.2 .

The 2HDISM consists of two doublets ϕ_1 and ϕ_2 and a real singlet S . The scalar potential of the model is

$$\begin{aligned} V(\phi_1,\phi_2,S) &= \mu_1^2\phi_1^\dagger\phi_1 + \mu_2^2\phi_2^\dagger\phi_2 - \mu_{12}^2\phi_1^\dagger\phi_2 - (\mu_{12}^2)^*\phi_2^\dagger\phi_1 \\ &+ \frac{\lambda_1}{2}\left(\phi_1^\dagger\phi_1\right)^2 + \frac{\lambda_2}{2}\left(\phi_2^\dagger\phi_2\right)^2 + \lambda_3\phi_1^\dagger\phi_1\phi_2^\dagger\phi_2 + \lambda_4\phi_1^\dagger\phi_2\phi_2^\dagger\phi_1 \\ &+ \frac{\lambda_5}{2}\left(\phi_1^\dagger\phi_2\right)^2 + \frac{\lambda_5^*}{2}\left(\phi_2^\dagger\phi_1\right)^2 \\ &- \phi_1^\dagger\phi_1\left(\lambda_6\phi_1^\dagger\phi_2 + \lambda_6^*\phi_2^\dagger\phi_1\right) - \phi_2^\dagger\phi_2\left(\lambda_7\phi_1^\dagger\phi_2 + \lambda_7^*\phi_2^\dagger\phi_1\right) \\ &- \mu_S^2S^2 + \frac{\lambda_S}{4}S^4 + \lambda_{S1}S^2\phi_1^\dagger\phi_1 \\ &+ \lambda_{S2}S^2\phi_2^\dagger\phi_2 + S^2\left(\frac{\lambda_{S12}}{2}\phi_1^\dagger\phi_2 + \frac{\lambda_{S12}^*}{2}\phi_2^\dagger\phi_1\right) \end{aligned} \tag{5.16}$$

and the VEVs of the doublets are

$$\langle\phi_1\rangle = \begin{pmatrix} 0 \\ \frac{\mathrm{e}^{\mathrm{i}\theta}v_1}{\sqrt{2}} \end{pmatrix} , \quad \langle\phi_2\rangle = \begin{pmatrix} 0 \\ \frac{v_2}{\sqrt{2}} \end{pmatrix} . \tag{5.17}$$

By transforming the ϕ_1 doublet with a $U(1)$ transformation $\phi_1 \to \mathrm{e}^{-\mathrm{i}\theta}\phi_1$ we can remove the phase of the VEV $\langle\phi_1\rangle$ and redefining the complex parameters $\mu_{12}, \lambda_5, \lambda_6, \lambda_7$ and λ_{S12} the form of the potential (5.16) is unchanged. Hence we just set $\theta = 0$. The VEV of the singlet S is set zero, $\langle S\rangle = 0$, because we consider it as a WIMP candidate.

From the minimum conditions

$$\partial_X\, V|_{\text{vacuum}} = 0 , \quad X = \phi_{1r}, \phi_{2r}, \phi_{1i}, \phi_{2i}, \phi_1^+, \phi_2^+, S , \tag{5.18}$$

we can solve $\mu_1,\ \mu_2$ and $\mathrm{Im}\mu_{12}^2 = \mu_{12i}^2$:

$$\begin{aligned} \mu_1^2 &= \frac{-v_1^3\lambda_1 + v_2\left(2\mu_{12r}^2 - v_1v_2\lambda_{345r} + 3v_1^2\lambda_{6r} + v_2^2\lambda_{7r}\right)}{2v_1} \\ \mu_2^2 &= \frac{-v_2^3\lambda_2 + v_1\left(2\mu_{12r} - v_1v_2\lambda_{345r} + v_1^2\lambda_{6r} + 3v_2^2\lambda_{7r}\right)}{2v_2} \\ \mu_{12i}^2 &= \frac{1}{2}\left(v_1v_2\lambda_{5i} - v_1^2\lambda_{6i} - v_2^2\lambda_{7i}\right) . \end{aligned} \tag{5.19}$$

The mass matrices of the neutral and charged sectors are symmetric 5×5 (N) and 2×2 (C) matrices, respectively, with elements

$$
\begin{aligned}
N_{11} &= \frac{v_2\left(2\mu_{12r}^2 - 2v_1v_2\lambda_{5r} + v_1^2\lambda_{6r} + v_2^2\lambda_{7r}\right)}{2v_1} \,, \\
N_{12} &= -\mu_{12r}^2 + v_1v_2\lambda_{5r} - \frac{1}{2}v_1^2\lambda_{6r} - \frac{1}{2}v_2^2\lambda_{7r} \,, \\
N_{13} &= \frac{1}{2}v_2\left(v_2\lambda_{5i} - 2v_1\lambda_{6i}\right) \,, \\
N_{14} &= \frac{1}{2}v_2\left(v_1\lambda_{5i} - 2v_2\lambda_{7i}\right) \,, \\
N_{22} &= \frac{v_1\left(2\mu_{12r}^2 - 2v_1v_2\lambda_{5r} + v_1^2\lambda_{6r} + v_2^2\lambda_{7r}\right)}{2v_2} \,, \\
N_{23} &= -\frac{1}{2}v_1v_2\lambda_{5i} + v_1^2\lambda_{6i} \,, \\
N_{24} &= -\frac{1}{2}v_1^2\lambda_{5i} + v_1v_2\lambda_{7i} \,, \\
N_{33} &= \frac{2v_1^3\lambda_1 + v_2\left(2\mu_{12r}^2 - 3v_1^2\lambda_{6r}\right) + v_2^3\lambda_{7r}}{2v_1} \,, \\
N_{34} &= -\mu_{12r}^2 + v_1v_2\lambda_{345r} - \frac{3}{2}v_1^2\lambda_{6r} - \frac{3}{2}v_2^2\lambda_{7r} \,, \\
N_{44} &= \frac{2v_2^3\lambda_2 + v_1^3\lambda_{6r} + v_1\left(2\mu_{12r}^2 - 3v_2^2\lambda_{7r}\right)}{2v_2} \,, \\
N_{51} &= N_{52} = N_{53} = N_{54} = 0 \,, \\
N_{55} &= 2\mu_S^2 + v_1v_2\lambda_{12r}^2 + v_1^2\lambda_{S1} + v_2^2\lambda_{S2} \,,
\end{aligned}
\tag{5.20}
$$

and

$$
\begin{aligned}
C_{11} &= \frac{v_2\left(2\mu_{12r}^2 - v_1v_2\lambda_{45r} + v_1^2\lambda_{6r} + v_2^2\lambda_{7r}\right)}{2v_1} \,, \\
C_{12} &= \frac{1}{2}\left(-2\mu_{12r}^2 + v_1v_2\lambda_{45r} - v_1^2\lambda_{6r} - v_2^2\lambda_{7r}\right) \,, \\
C_{22} &= \frac{v_1\left(2\mu_{12r}^2 - v_1v_2\lambda_{45r} + v_1^2\lambda_{6r} + v_2^2\lambda_{7r}\right)}{2v_2} \,,
\end{aligned}
\tag{5.21}
$$

in bases $\{\phi_{1i}, \phi_{2i}, \phi_{1r}, \phi_{2r}, S\}$ and $\{\phi_1^+, \phi_2^+\}$, respectively. As we can see from the mass matrix of the neutral fields, there is mixing between the real and imaginary parts of the neutral fields. That is, the mass eigenstates are not CP eigenstates, which provides a source for CP violation. As the VEV of the singlet S is zero, it does not mix with the other scalar fields and as a result, it does not decay. Hence it may be a potential WIMP candidate. Remaining

4×4 mass matrix can be diagonalized with the rotation

$$R_4 = \begin{pmatrix} 1 & 0 & 0 & 0 \\ 0 & c_y c_z & -c_y s_z & s_y \\ 0 & s_x s_y c_z + c_x s_z & c_x c_z - s_x s_y s_z & -s_x c_y \\ 0 & s_x s_z - c_x s_y c_z & c_x s_y s_z + s_x c_z & c_x c_y \end{pmatrix} \begin{pmatrix} c_\beta & s_\beta & 0 & 0 \\ -s_\beta & c_\beta & 0 & 0 \\ 0 & 0 & 1 & 0 \\ 0 & 0 & 0 & 1 \end{pmatrix} , \tag{5.22}$$

and we arrange the mass eigenbasis such that

$$\begin{pmatrix} G_0 \\ A_0 \\ H \\ h \end{pmatrix} = R_4 \begin{pmatrix} \phi_{1i} \\ \phi_{2i} \\ \phi_{1r} \\ \phi_{2r} \end{pmatrix} . \tag{5.23}$$

Similarly as in the 2HDM the charged sector is diagonalized with the rotation

$$R_2 = \begin{pmatrix} \cos\beta & \sin\beta \\ -\sin\beta & \cos\beta \end{pmatrix} , \quad \tan\beta = \frac{v_2}{v_1} , \tag{5.24}$$

and the mass eigenstates are

$$\begin{pmatrix} G^+ \\ H^+ \end{pmatrix} = R_2 \begin{pmatrix} \phi_1^+ \\ \phi_2^+ \end{pmatrix} . \tag{5.25}$$

Here G_0 and G^+ are the neutral and charged Goldstone bosons.

5.3 Theoretical constraints

The scalar potential (5.16) includes 20 free parameters, three of which are fixed by the minimum conditions (5.19) . Also the angle β is a free parameter. So the 2HDISM includes all in all $20 - 3 + 1 = 18$ free parameters. We would like to constrain the parameter space of the 2HDISM. Let us first find out theoretical constraints for the model.

Most obvious theoretical constraints arise from the vacuum stability requirement [61] . To calculate the vacuum stability constraints it is convenient to write the doublets as

$$\phi_1 = \begin{pmatrix} \phi_5 + \mathrm{i}\phi_6 \\ \phi_1 + \mathrm{i}\phi_2 \end{pmatrix} , \quad \phi_2 = \begin{pmatrix} \phi_7 + \mathrm{i}\phi_8 \\ \phi_3 + \mathrm{i}\phi_4 \end{pmatrix} . \tag{5.26}$$

For instance, along the direction where $\phi_j = 0$ for all $j \neq 1$ and $S = 0$ the potential behaves as $\lambda_1 \phi_1^4 / 2$ for large ϕ_1 . This gives a constraint $\lambda_1 \geq 0$.

Similarly along the direction where only ϕ_1 and ϕ_7 are non-zero the potential behaves as

$$\frac{\lambda_1}{2}\phi_1^4 + \frac{\lambda_2}{2}\phi_7^4 + \lambda_3\phi_1^2\phi_7^2 \,. \tag{5.27}$$

Writing $\phi_1 = r\cos\delta$, $\phi_7 = r\sin\delta$ we get from the boundedness requirement that

$$\frac{\lambda_1}{2}\cos^4\delta + \frac{\lambda_2}{2}\sin^4\delta + \lambda_3\cos^2\delta\sin^2\delta \geq 0 \,, \tag{5.28}$$

for all $\delta \in [0, \pi/2]$. Minimizing the left hand side of the equation (5.28) gives a simple bound $\lambda_3 \geq -\sqrt{\lambda_1\lambda_2}$. Considering all the different simple cases, where we vary only two fields keeping the other fields zero, we get the following constraints:

$$\begin{aligned}
&\lambda_{1,2,S} \geq 0 \,, \;\; \lambda_3 \geq -\sqrt{\lambda_1\lambda_2} \,, \\
&\lambda_{1S} \geq -\sqrt{\frac{\lambda_1\lambda_S}{2}} \,, \;\; \lambda_{2S} \geq -\sqrt{\frac{\lambda_2\lambda_S}{2}} \,, \\
&|\lambda_{6r} + \lambda_{7r}| \leq \frac{1}{4}(\lambda_1 + \lambda_2) + \frac{1}{2}(\lambda_3 + \lambda_4 + \lambda_{5r}) \,, \\
&|\lambda_{6i} + \lambda_{7i}| \leq \frac{1}{4}(\lambda_1 + \lambda_2) + \frac{1}{2}(\lambda_3 + \lambda_4 - \lambda_{5r}) \,,
\end{aligned} \tag{5.29}$$

and from the last two constraints in equation (5.29) it follows that

$$\begin{aligned}
&\lambda_3 + \lambda_4 + \frac{1}{2}(\lambda_1 + \lambda_2) \geq 0 \,, \\
&|\lambda_{5r}| \leq \lambda_3 + \lambda_4 + \frac{1}{2}(\lambda_1 + \lambda_2) \,.
\end{aligned} \tag{5.30}$$

Moreover, the vacuum stability and conditions (5.19) are not enough to ensure the global minimum as the VEV of the singlet S is zero. If there is a minimum where $S = w \neq 0$, then from the condition $\partial_S V|_{\text{minimum}} = 0$ we can solve w :

$$w^2 = -\frac{2\mu_S^2 + 2v_1v_2\lambda_{S12r} + v_1^2\lambda_{S1} + v_2^2\lambda_{S2}}{\lambda_S} \,. \tag{5.31}$$

Now we require that the minimum where $S = 0$ is the global minimum, so

$$V|_{\text{min}_0} < V|_{\text{min}_w} \,, \tag{5.32}$$

where min_0 and min_w correspond to the minima where $S = 0$ and $S = w$, respectively. The condition (5.32) can be written as

$$\left|m_S^2\right| < v_1v_2\lambda_{S12r} + \frac{1}{2}v_1^2\lambda_{S1} + \frac{1}{2}v_2^2\lambda_{S2} \,. \tag{5.33}$$

In the Monte Carlo calculation we will take into account all vacuum stability constraints. To do that we write the potential in spherical coordinates

$$\begin{aligned} \phi_k &= r \cos\delta_k \prod_{j=1}^{k-1} \sin\delta_j \\ S &= r \prod_{j=1}^{8} \sin\delta_j \ . \end{aligned} \tag{5.34}$$

For large r the fourth order terms are dominant, thus the vacuum stability condition is

$$\min\left(\lim_{r\to\infty} \frac{V(r,\delta_j)}{r^4} \right) > 0 \ . \tag{5.35}$$

where the minimum is taken over all angles δ_j .

More constraints can be set by requiring tree level unitarity [62, 63] . The unitarity requirement reduces to a constraint on the quadratic coupling and can be written as a upper limit on the eigenvalues Λ_j of the $2 \to 2$ scattering matrix: $|\Lambda_j| < 8\pi$. By diagonalizing scattering matrices corresponding to the sets of states

$$\begin{aligned} &\{\phi_{1r}\phi_{2r}, \phi_{1i}\phi_{2i}, \phi_{1r}\phi_{2i}, \phi_{1i}\phi_{2r}, \phi_1^-\phi_2^+, \phi_1^+\phi_2^-\} \ , \\ &\{\phi_{1r}\phi_{1r}, \phi_{1i}\phi_{1i}, \phi_{2r}\phi_{2r}, \phi_{2i}\phi_{2i}, \phi_1^-\phi_1^+, \phi_2^-\phi_2^+\} \end{aligned} \tag{5.36}$$

we obtain the following simple constraints:

$$|\lambda_1 + \lambda_2| < 8\pi \ , \ \ |\lambda_3 + \lambda_4| < 8\pi \ , \ \ |\lambda_{5r}| < \sqrt{(4\pi + \lambda_1)(4\pi + \lambda_2)} \ . \tag{5.37}$$

These constraints are necessary but not sufficient for the unitarity requirement. In principle we should diagonalize the full scattering matrix including also S and gauge bosons. In the Monte Carlo calculation we ensure the unitarity by diagonalizing the full scattering matrix numerically.

5.4 Oblique constraints

We would like to know if the model is consistent with the electroweak precision data. For this purpose we use oblique parameters introduced by Peskin and Takeuchi [64]. The oblique parameters are S, T, and U and their higher order extensions V, W, and X [65] . These parameters quantify deviations of electroweak precision data from the SM. Parameters S , T and U can be used to constrain effects of new physics if the following criteria are satisfied [65]:

1. The electroweak gauge group is $\mathrm{SU(2)_L} \times \mathrm{U(1)_Y}$.

2. Couplings of new particles to light fermions are suppressed compared to their couplings to the gauge bosons.

3. The mass scale of the new physics is (much) larger than M_Z .

If the third criterion is not satisfied, then also the higher order extensions V, W, and X should be used.

We assume that our model satisfies all the three criteria and for simplicity we use only S and T parameters. This may constrain the model too strongly, but at least the parameter sets satisfying these constraints are consistent with the electroweak precision data. The experimental values for S and T are [66]

$$S = 0.04 \pm 0.09 \ , \quad T = 0.07 \pm 0.08 \tag{5.38}$$

with correlation between the experimental fits for S and T is $\rho = 0.88$. In SM the values for S and T are fixed to $S = T = 0$ for the reference Higgs mass $115.5\,\mathrm{GeV} < m_h < 127\,\mathrm{GeV}$ [66] .The SM predictions for the oblique parameters are well consistent with the experimental values, thus the corrections from physics beyond the SM should be small.

The 1σ, 2σ and 3σ regions are ellipses in the ST -plane as shown in figure 5.1 . The rotation angle is

$$\theta = \frac{1}{2} \arctan\left(\frac{2\rho\,\delta S\,\delta T}{\delta S^2 - \delta T^2} \right) \ , \tag{5.39}$$

and lengths of the semi axes a_k, b_k satisfy the equations

$$\begin{aligned} \frac{(\rho\,\delta T\cos\theta - \delta S\sin\theta)^2}{b_k^2} + \frac{(\delta S\cos\theta + \rho\,\delta T\sin\theta)^2}{a_k^2} &= \frac{1}{\delta_k} \ , \\ -\frac{\delta T^2\,(-1+\rho^2)\left(a_k^2\cos^2\theta + b_k^2\sin^2\theta\right)}{a_k^2\,b_k^2} &= \frac{1}{\delta_k} \ , \end{aligned} \tag{5.40}$$

where $\delta_1 = 2.3$, $\delta_2 = 6.18$ and $\delta_3 = 11.83$ correspondint to 1σ , 2σ and 3σ CLs.

In the reference [67] expressions for the S and T parameters are calculated for a model with an arbitrary number of doublets and singlets in terms of the masses and mass eigenstates. For the 2HDM with one singlet these can be

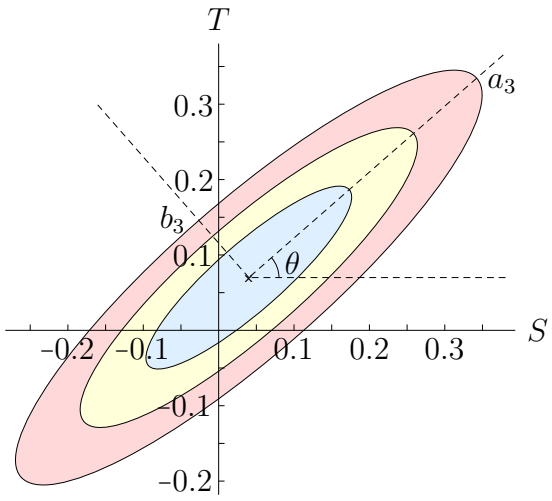

Figure 5.1. 1σ (blue), 2σ (yellow) and 3σ (red) CL regions of the oblique parameters S and T .

written as

$$\begin{aligned} S = \frac{1}{24\pi}\Bigg(& 2s_W^2 - (U^\dagger U)_{2,2})^2 G(m_{H^+}^2, m_{H^+}^2, M_Z^2) \\ & - 2(U^\dagger U)_{2,2} \ln(m_{H^+}^2) - \ln(m_h^2) - G_h(m_h^2, M_Z^2) \\ & + \sum_{b=2}^{4} \sum_{b'=b+1}^{5} (\mathrm{Im}(V^\dagger V)_{b,b'})^2 G(m_{N,b}^2, m_{N,b'}^2, M_Z^2) \\ & + \sum_{b=2}^{5} \left((V^\dagger V)_{b,b} \ln(m_{N,b}^2) + (\mathrm{Im}(V^\dagger V)_{1,b})^2 G_h(m_{N,b}^2, M_Z^2) \right) \Bigg) \end{aligned} \tag{5.41}$$

and

$$\begin{aligned} T = \frac{1}{16\pi s_W^2 M_W^2}\Bigg(& \sum_{b=2}^{5} \left| (U^\dagger V)_{2,b} \right|^2 F(m_{H^+}^2, m_{N,b}) \\ & - \sum_{b=2}^{4} \sum_{b'=b+1}^{5} \mathrm{Im}((V^\dagger V)_{b,b'})^2 F(m_{N,b}^2, m_{N,b'}^2) \\ & + 3 \sum_{b=2}^{5} (\mathrm{Im}(V^\dagger V)_{1,b})^2 (F(M_Z^2, m_{N,b}^2) - F(M_W^2, m_{N,b}^2)) \\ & - 3(F(M_Z^2, m_h^2) - F(M_W^2, m_h^2)) \Bigg) , \end{aligned} \tag{5.42}$$

where

$$m_N = (0, m_{A_0}, m_H, m_S, m_h) \, . \tag{5.43}$$

The matrices U and V are defined so that U diagonalizes the charged sector,

$$UM_C^2U^\dagger = \mathrm{diag}(0, m_{H^+}^2) \ , \tag{5.44}$$

and $V = (\tilde{V}_1, \tilde{V}_2) + \mathrm{i}(\tilde{V}_3, \tilde{V}_4)$, where the lower indices refer to the rows of the matrix $\tilde{V}$, diagonalizes the neutral sector,

$$\tilde{V}M_N^2\tilde{V}^\dagger = \mathrm{diag}(0, m_{A_0}^2, m_H^2, m_S^2, m_h^2) \ . \tag{5.45}$$

Note that the summations in the formulae (5.42) and (5.41) explicitly leave out the Goldstone modes. Functions G, G_h and F are defined as

$$\begin{aligned} G(x,y,z) = &-\frac{16}{3} + 5\frac{x+y}{z} - 2\frac{(x-y)^2}{z^2} \\ &+ \frac{z^2 - 2z(x+y) + (x-y)^2)}{z^3} \\ &\cdot f(x+y-z, z^2 - 2z(x+y) + (x-y)^2) \\ &+ \begin{cases} \frac{3}{z}(\frac{x^2+y^2}{x-y} - \frac{x^2-y^2}{z} + \frac{(x-y)^3}{3z^2})\ln\frac{x}{y} \ , & x \neq y \ , \\ 6\frac{y}{z} \ , & x = y \ , \end{cases} \end{aligned} \tag{5.46}$$

$$G_h(x,y) = G(x,y,y) + 12G_t(x,y,y) \tag{5.47}$$

and

$$F(x,y) = \begin{cases} \frac{x+y}{2} - \frac{xy}{x-y}\ln\frac{x}{y} \ , & x \neq y \ , \\ 0 \ , & x = y \ , \end{cases} \tag{5.48}$$

where

$$f(t,r) = \begin{cases} \sqrt{r}\ln\left|\frac{t-\sqrt{r}}{t+\sqrt{r}}\right| \ , & r > 0 \ , \\ 0 \ , & r = 0 \ , \\ 2\sqrt{-r}\arctan\frac{\sqrt{-r}}{t} \ , & r < 0 \ , \end{cases} \tag{5.49}$$

and

$$G_t(x,y,z) = \begin{cases} -2 + (\frac{x-y}{z} - \frac{x+y}{x-y})\ln\frac{x}{y} + \frac{f(x+y-z, z^2-2z(x+y)+(x-y)^2)}{z} \ , & x \neq y \ , \\ -4 + \frac{f(2x-z, z^2-4zx)}{z} \ , & x = y \ . \end{cases} \tag{5.50}$$

5.5 Monte Carlo analysis

Now we constrain the 2HDISM with the Higgs decay data. To do that we need expressions for the parameters a_f and a_V in terms of the rotation angles β and $\alpha_{x,y,z}$. The coupling of the Higgs boson h to fermions is

$$\frac{m_f \cos\alpha_x \cos\alpha_y}{v \sin\beta} \tag{5.51}$$

whereas in the SM the coupling is m_f/v , thus

$$a_f = \frac{\cos\alpha_x \cos\alpha_y}{\sin\beta} \ . \tag{5.52}$$

Similarly

$$a_V = \cos\alpha_x(\sin\alpha_y \sin\alpha_z \cos\beta + \cos\alpha_y \sin\beta) + \sin\alpha_x \cos\alpha_z \cos\beta \ . \tag{5.53}$$

But there are also charged scalar bosons $H^\pm$ in the model, so we should include the term

$$-a_S \frac{2m_{H^+}^2}{v} h H^+ H^- \tag{5.54}$$

to the effective Lagrangian (2.16) . The hH^+H^- coupling affects the $h \to \gamma\gamma$ channel, because the charged scalar boson interacts with photons, so the Higgs boson can decay to two photons via H^+ loop. In order to take the H^+ loop into account we use the formula given in [26] :

$$\Gamma_{\gamma\gamma}(a_f, a_V, a_S) = \frac{\alpha^2 g^2 m_h^3}{1024\pi^3 M_W^2} \left| \frac{4}{3} a_f F_{1/2} + a_V F_1 + a_S F_0 \right|^2 \ , \tag{5.55}$$

where

$$F_0 = \frac{4m_{H^+}^2}{m_h^2} \left(1 - \frac{4m_{H^+}^2}{m_h^2} f\left(\frac{4m_{H^+}^2}{m_h^2} \right) \right) \ , \tag{5.56}$$

and the functions $F_1, F_{1/2}$ and f are given by the formulae (2.26) and (2.27) . The χ^2 fit is not very sensitive to the mass of the H^+ boson, so for the χ^2 fit we use $m_{H^+} = 4\,\mathrm{TeV}$. Now

$$G_{\gamma\gamma} \approx 0.0238 \left(1.84 a_f + 0.33 a_S - 8.32 a_V\right)^2 \ . \tag{5.57}$$

We also need the expression for the a_S parameter:

$$\begin{aligned} a_S = \big[& s_\beta c_\beta v^2 \left(\lambda_1 c_\beta^3 (-(c_x s_y s_z + s_x c_z)) - \lambda_3 c_x s_y s_z s_\beta^2 c_\beta + \lambda_4 c_x s_y s_z s_\beta^2 c_\beta \right. \\ & -\lambda_3 c_x c_y s_\beta c_\beta^2 + \lambda_4 c_x c_y s_\beta c_\beta^2 - \lambda_2 c_x c_y s_\beta^3 - \lambda_3 s_x c_z s_\beta^2 c_\beta + \lambda_4 s_x c_z s_\beta^2 c_\beta \\ & -2 c_x s_y c_z s_\beta^2 c_\beta^2 \lambda_{5i} + 2 s_x s_z s_\beta^2 c_\beta^2 \lambda_{5i} - 2 c_x s_y c_z s_\beta c_\beta^3 \lambda_{6i} + 2 s_x s_z s_\beta c_\beta^3 \lambda_{6i} \\ & -2 c_x s_y c_z s_\beta^3 c_\beta \lambda_{7i} + 2 s_x s_z s_\beta^3 c_\beta \lambda_{7i} + c_x s_y s_z s_\beta^2 c_\beta \lambda_{5r} + c_x c_y s_\beta c_\beta^2 \lambda_{5r} \\ & +s_x c_z s_\beta^2 c_\beta \lambda_{5r} - c_x s_y s_z s_\beta c_\beta^2 \lambda_{6r} + c_x c_y c_\beta^3 \lambda_{6r} - s_x c_z s_\beta c_\beta^2 \lambda_{6r} \\ & \left. +s_\beta^2 \lambda_{7r} (c_x s_y s_z s_\beta - c_x c_y c_\beta + s_x c_z s_\beta) \right) \big] \\ & \cdot \left[2\mu_{12r}^2 + v^2 \left(c_\beta \left(c_\beta \lambda_{6r} - s_\beta \left(\lambda_4 + \lambda_{5r} \right) \right) + s_\beta^2 \lambda_{7r} \right) \right]^{-1} \ . \end{aligned} \tag{5.58}$$

Scalar bosons H and A_0 do not affect the Higgs decay, because they are much heavier than the Higgs boson. The mass of the singlet S might be less than half of the Higgs mass, which would enable the invisible decay channel $h \to SS$. We studied the invisible decay channel already in the section 4.1 and saw that it is disfavored by the Higgs decay data.

Next we scan the 18 dimensional parameter space looking for points that satisfy the theoretical constraints as well as the constraints arising from the electroweak precision data and Higgs decay data. We consider only lambda parameter values $|\lambda_j| < \pi$, in order to maintain perturbativity, so the simplest unitarity constraints (5.37) are automatically fulfilled. Moreover we fix one of the parameters, μ_{12r} , by the Higgs boson mass $m_h = 125\,\mathrm{GeV}$, require that the masses of the new scalar bosons are sufficiently large [68, 69] :

$$m_H, m_{A_0} > 600\,\mathrm{GeV}\ , \quad m_{H^+} > 100\,\mathrm{GeV}\ . \tag{5.59}$$

and concentrate on the mass region $m_S < 200\,\mathrm{GeV}$. So, we randomly generate parameter sets using constraints $|\lambda_j| < \pi$, (5.29) and (5.33) as bounds, diagonalize the mass matrices numerically and calculate S and T values using formulae (5.41) and (5.42) for those parameter sets which satisfy the mass bounds (5.59) . Distribution in the (S, T) plane together with 1σ , 2σ and 3σ CL regions is shown in figure 5.2.

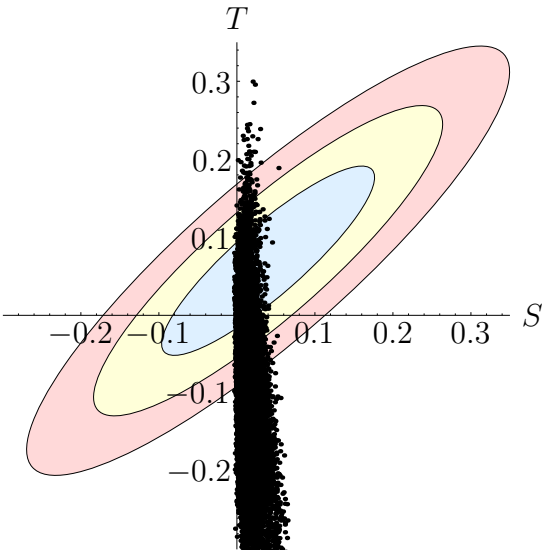

Figure 5.2. Randomly generated points of the 2HDISM together with the 1σ (blue), 2σ (yellow) and 3σ (red) CL regions in the (S, T) plane. Higgs decay constraints and complete unitary and vacuum stability constraints are not yet considered.

Then we calculate a_f , a_V and a_S values using formulae (5.52) , (5.53) and (5.58) , taking only those points which hit inside the 2σ region in the (S, T)

plane. Figure 5.3 shows how these points are distributed. As expected, we obtain only a_V values less than one, since the mixing between h , H and A_0 reduces the gauge boson couplings. Note that the parameter space points are distributed strictly around $a_S = 0$. Hence to constrain the parameter space we consider the plane that passes through the SM point $(a_f, a_V, a_S) = (1, 1, 0)$. We accept only points which are inside the 2σ region in plot 5.3b .

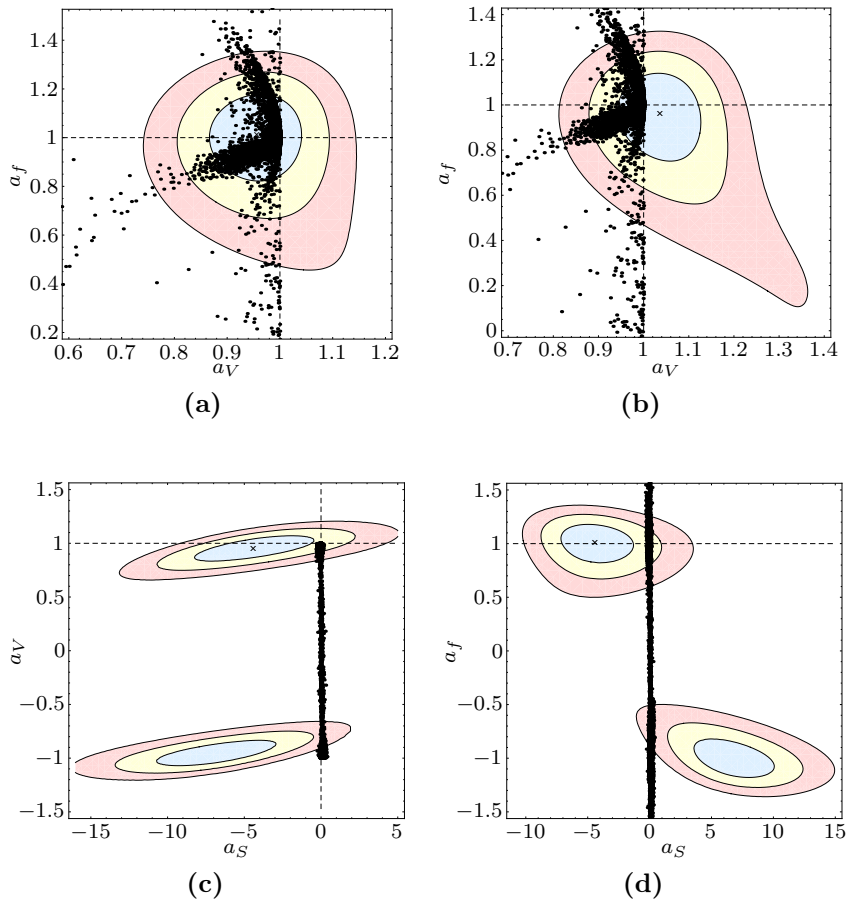

Figure 5.3. Higgs decay data fit for the 2HDISM. Black points are the parameter space points, which satisfy the 2σ ST bounds and the simplest vacuum stability constraints. Blue, red and yellow areas correspond to the 1σ, 2σ and 3σ CL regions, respectively. Plots (a), (c) and (d) are the intersections through the best fit point $(a_f, a_V, a_S) = (1.02, 0.96, -4.42)$. Plot (b) shows the fit at $a_S = 0$.

Finally, we check that the complete unitarity and vacuum stability constraints are fulfilled. This is the slowest part of the calculation so we want to constrain the parameter space as much as possible before calculating the

complete unitarity and vacuum stability constraints. The vacuum stability and unitarity constraints decrease the number of acceptable points drastically. Figure 5.4 shows how the vacuum stability and unitarity requirements constrain the parameter space and in figure 5.5 distributions of the masses and mixing angles are shown.

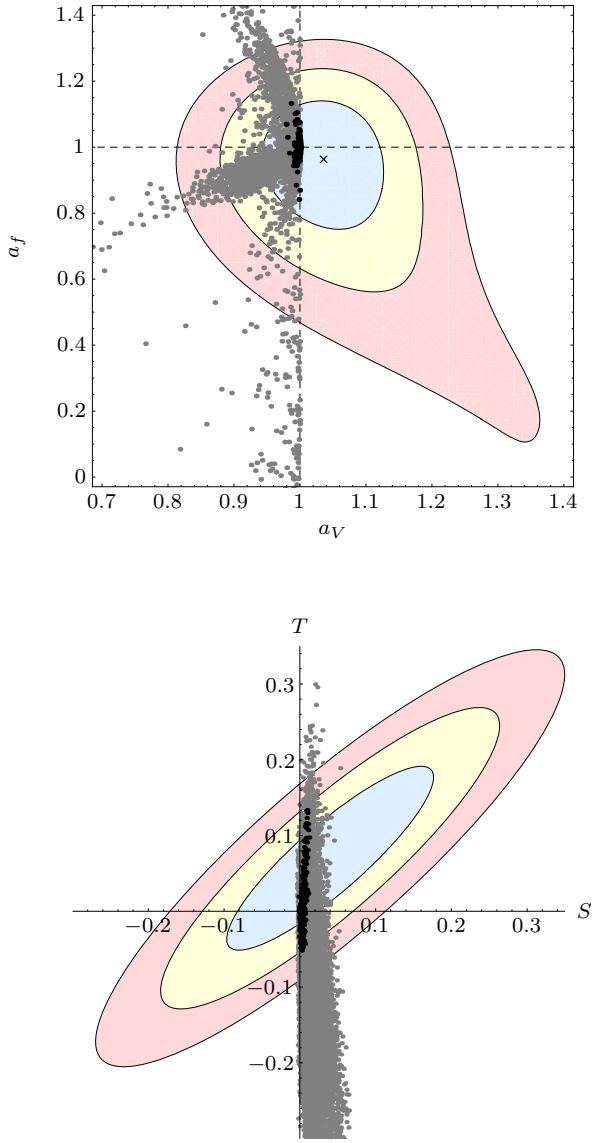

Figure 5.4. Viable points in the (a_f, a_V) and (S, T) planes together with the 1σ (blue), 2σ (yellow) and 3σ (red) CL regions. For the black points the full vacuum stability and unitarity constraints are taken into account as well as the 2σ ST bounds and the 2σ constraints from the Higgs decay data.

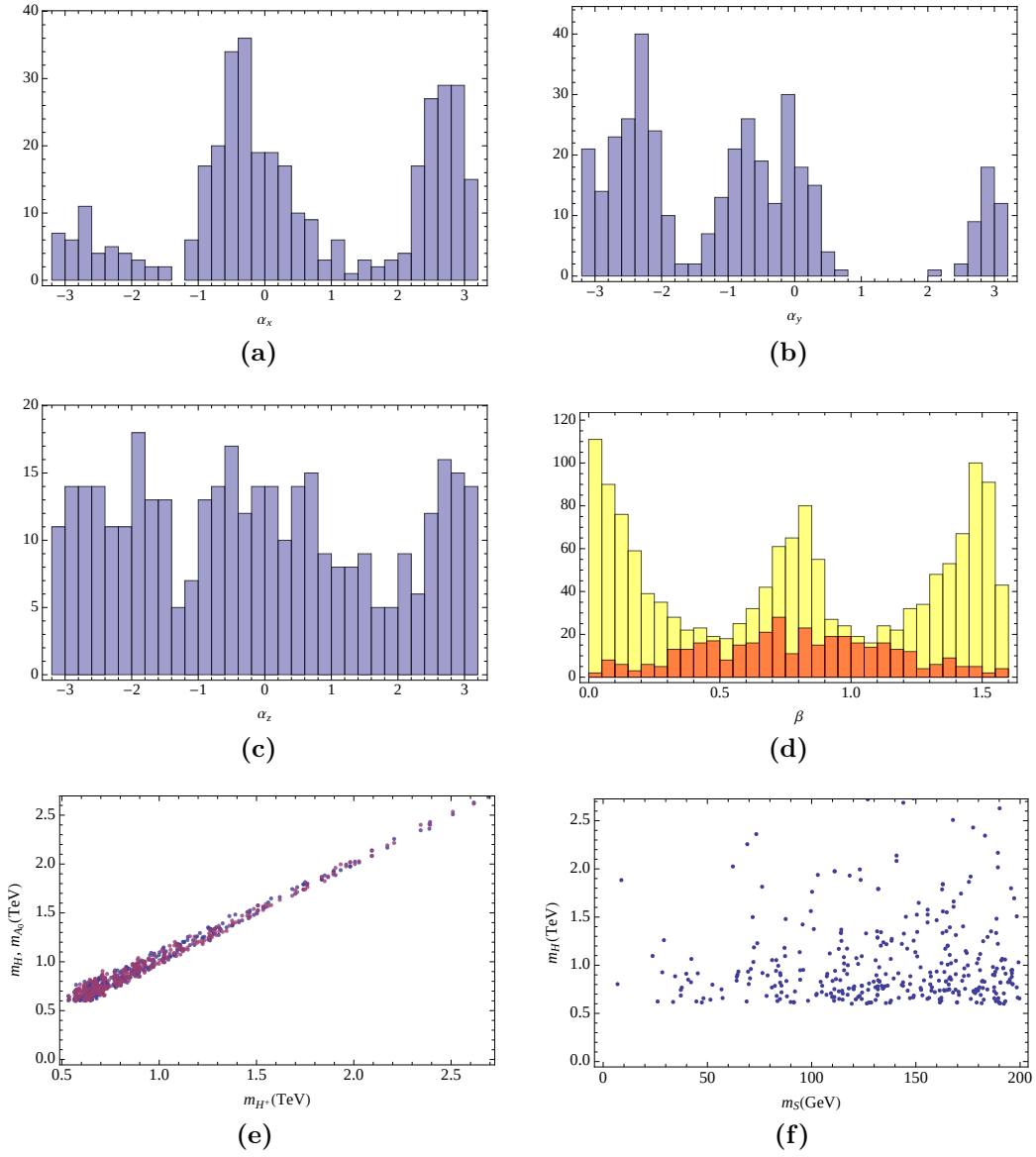

Figure 5.5. (a),(b),(c): Rotation angles α_x , α_y and α_z corresponding to points which satisfy all constraints. (d): Parameter β before (yellow, scaled) and after (red) the Higgs decay and full vacuum stability and unitarity constraints. Plots (e) and (f) show the distributions of the masses of the new scalar bosons.

5.6 Dark matter relic abundance

Using formulae given in the appendix C we calculate the annihilation cross-section for the dark matter candidate S . The annihilation channels are

$$\begin{gathered} SS \to hh \ , \ \ SS \to HH \ , \ \ SS \to A_0 A_0 \ , \\ SS \to hH \ , \ \ SS \to hA_0 \ , \ \ SS \to HA_0 \ , \ \ SS \to H^+ H^- \ , \\ SS \to W^+ W^- \ , \ \ SS \to ZZ \ , \ \ SS \to f\overline{f} \ . \end{gathered} \tag{5.60}$$

Similarly as in the section 4.2 we now calculate the relic abundance taking into account only points which satisfy the 2σ ST bounds and the 2σ constraints from the Higgs decay data, and survive the complete vacuum stability and unitarity constraints. Relative relic abundance for these points is shown in figure 5.6 .

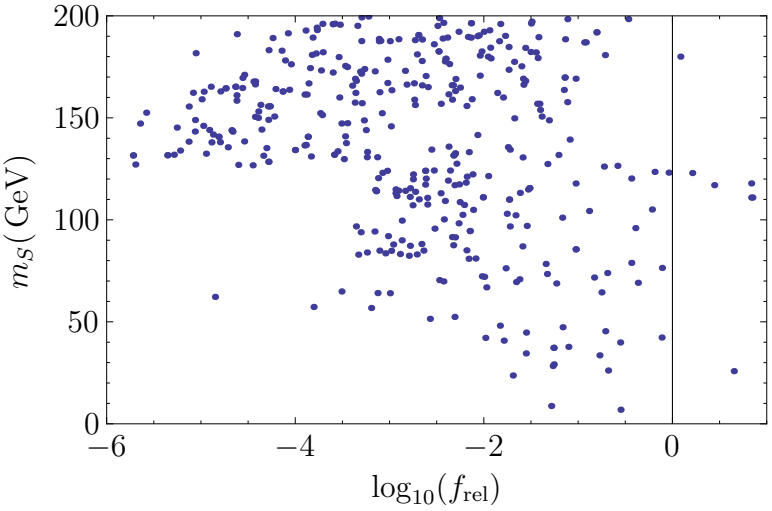

Figure 5.6. Logarithm of $f_{\rm rel} = \Omega h^2/0.12$ for different dark matter candidate masses m_S .

From figure 5.6 we see that there are potential points in the parameter space producing a dark matter candidate, that may account for a significant amount of the total dark matter mass density. To proceed we could take for example those points which may account for more than 1% of the total dark matter mass density and check if they could provide required conditions for the baryogenesis. We could also check how the constraints from the direct and indirect dark matter searches would constrain the parameter space and up to how large energies the model could maintain perturbativity and vacuum stability. The work in order to take these constraints into account is in progress [70] .

Chapter 6

Conclusions

In this thesis we have studied the SM Higgs sector and compared it to the latest data from the LHC and Tevatron experiments. We considered a modified Lagrangian to study how much the Higgs boson couplings to the electroweak gauge bosons and fermions can deviate from the SM. We concluded that the SM is well in agreement with the Higgs boson measurements.

Then we considered two extensions of the Higgs sector. First we extended the SM Higgs sector with one real singlet. We studied the invisible decay channel of the Higgs boson and noticed that it significantly constraints the parameter space in the region where the mass of the singlet is less than half of the Higgs boson mass. The singlet could provide a good dark matter candidate, so we also calculated its relic abundance.

Finally we examined the two-Higgs-doublet model extended with one real singlet. We carried out Monte Carlo analysis of the model constraining the parameter space with vacuum stability and unitarity requirements as well as with electroweak precision data and Higgs decay data. Again we considered the singlet as a dark matter candidate and calculated its relic abundance. According to our analysis, there are potential regions in the parameter space which fulfill both the theoretical and experimental constraints, and provide a dark matter candidate which could constitute significant amount of the total dark matter mass density. Checking the conditions for the baryogenesis and taking into account the constraints from the direct and indirect dark matter searches and from perturbativity and vacuum stability at high energies is left for future work.

Appendix A

Summary of statistics

This is a brief summary of statistics needed in this thesis. For a more complete review see for example chapters 35 and 36 of the reference [66] .

Experiments in particle physics, when searching for new particles, are looking for excesses over the expected background. Hence a discovery requires being convinced that the excess is not a statistical fluctuation of the background. Usually particle physicists talk about a discovery when the significance of the observation is more than 5σ . This means that assuming a Gaussian distribution,

$$f_G(x) = \frac{1}{\sqrt{2\pi}\sigma} \mathrm{e}^{-(x-\mu)^2/2\sigma^2} \ , \tag{A.1}$$

for the statistical fluctuations of the background the excess is more than 6 standard deviations σ from the expectation value μ of the background. So if the significance of the observation is $z\sigma$ the probability that the observed excess arises from the fluctuations of the background is

$$\alpha = 1 - \int_{\mu-z\sigma}^{\mu+z\sigma} f_G(x)\mathrm{d}x = 1 - \mathrm{erf}\left(\frac{z}{\sqrt{2}}\right) \ , \tag{A.2}$$

which for $z = 5$ is $\alpha = 5.73 \cdot 10^{-7}$.

Let us suppose that we have N independent Gaussian random variables. That is, we have a set of N measurements with expectation values μ_i and variances σ_i^2 . The probability of finding a set $\{x_i(\{\theta_j\})\}$, depending on M parameters $\{\theta_j\}$, such that $x_i(\{\theta_j\}) \in [\mu_i - \mathrm{d}x, \mu_i + \mathrm{d}x]$ for all i is simply

$$L(\{\theta_j\}) = 2\prod_{i=1}^{N} \frac{1}{\sqrt{2\pi}\sigma_i} \mathrm{e}^{-(x_i(\{\theta_j\})-\mu_i)^2/2\sigma_i^2} \mathrm{d}x \ . \tag{A.3}$$

Table A.1. Values of $|\chi^2(\{\theta_j\}) - \chi^2(\{\hat{\theta}_j\})|$ for M parameters for different confidence levels β .

β	$M=1$	$M=2$	$M=3$
0.6827	1.00	2.30	3.53
0.9545	4.00	6.18	8.02
0.9973	9.00	11.83	14.16

Now the set of parameters $\{\theta_j\}$ describing best the measurements is the set which maximizes L , or equally the set that minimizes

$$\begin{aligned}\chi^2(\{\theta_j\}) &= -2\left(\ln\left(\frac{L(\{\theta_j\})}{\mathrm{d}x}\right) - \ln\left(2\prod_{i=1}^{N}\frac{1}{\sqrt{2\pi}\sigma_i}\right)\right) \\ &= \sum_{i=1}^{N}\frac{(x_i(\{\theta_j\}) - \mu_i)^2}{\sigma_i^2} \ .\end{aligned} \tag{A.4}$$

The method of finding best fit values $\hat{\theta}_j$ for parameters θ_j by minimizing $\chi^2(\{\theta_j\})$ is known as the method of least squares.

In general, if we have n independent Gaussian distributed variables having mean μ_i and variances σ_i^2 , then

$$z = \sum_{i=1}^{n}\frac{(x_i - \mu_i)^2}{\sigma_i^2} \tag{A.5}$$

is distributed according to chi-squared distribution

$$f_{\chi^2}(z,n) = \frac{z^{n/2-1}\mathrm{e}^{-z/2}}{2^{n/2}\Gamma(n/2)} \ . \tag{A.6}$$

Hence limits on the parameters θ_j at confidence level β can be obtained by requiring

$$\int_0^{\Delta\chi^2} f_{\chi^2}(z,M)\mathrm{d}z = \beta \ , \tag{A.7}$$

where $\Delta\chi^2 = |\chi^2(\{\theta_j\}) - \chi^2(\{\hat{\theta}_j\})|$. In table A.1 we have calculated the values of the difference $\Delta\chi^2$ in the cases $M = 1, 2, 3$ for confidence levels 0.6827 , 0.9545 and 0.9973 , which correspond to the 1σ , 2σ and 3σ limits for Gaussian distribution, respectively.

Appendix B

Solution of the Lee-Weinberg equation

Decoupling of the dark matter particles S (WIMPs) from the visible matter is described by the Lee-Weinberg equation

$$\frac{\mathrm{d}n}{\mathrm{d}t} = -3Hn + \langle v\sigma \rangle \left(n_{\mathrm{eq}}^2 - n^2 \right) \ , \tag{B.1}$$

where H is the Hubble parameter, n is the particle number density of the WIMPs, n_{eq} is the particle number density in the thermal equilibrium and $\langle v\sigma \rangle$ is the flux-weighted thermally averaged annihilation cross-section of the WIMPs. The equilibrium number density is

$$n_{\mathrm{eq}} = g \int \frac{\mathrm{d}^3 p}{(2\pi)^3} f(p,T) \tag{B.2}$$

where g is the number of intrinsic degrees of freedom for the WIMP and $f(p,T)$ is the equilibrium distribution function, which at low temperatures can be approximated as

$$f(p,T) = \mathrm{e}^{-E/T} \ . \tag{B.3}$$

Hence the equilibrium number density is

$$n_{\mathrm{eq}} = \frac{g}{2\pi^2} \int_m^\infty E\sqrt{E^2 - m_S^2}\, \mathrm{e}^{-E/T} \mathrm{d}E = \frac{g m_S^2 T}{2\pi^2} K_2 \left(\frac{m_S}{T} \right) \ . \tag{B.4}$$

Under the assumption (B.3) the flux-weighted thermally averaged annihilation cross-section,

$$\langle v\sigma \rangle = \frac{\int \mathrm{d}^3 p_1 \mathrm{d}^3 p_2 f(p_1,T) f(p_2,T) v\sigma}{\int \mathrm{d}^3 p_1 \mathrm{d}^3 p_2 f(p_1,T) f(p_2,T)} \tag{B.5}$$

where

$$v = \sqrt{\frac{(p_1 \cdot p_2)^2 - (m_1 m_2)^2}{(p_1^2 + m_1^2)(p_2^2 + m_2^2)}} \,, \tag{B.6}$$

can be written as [71]

$$\langle v\sigma \rangle = \frac{1}{8 m_S^4 T K_2^2 \left(\frac{m_S}{T}\right)} \int\limits_{4m_S^2}^{\infty} \mathrm{d}s \sqrt{s}(s - 4m_S^2) K_1 \left(\frac{\sqrt{s}}{T}\right) \sigma_{tot}(s) \,. \tag{B.7}$$

In the equations (B.4) and (B.7) K_n are the modified Bessel functions of second kind. In the radiation dominated Universe the Hubble parameter is

$$H^2 = \frac{8\pi}{3 M_{\text{Planck}}^2} \rho_{\text{tot}} = \frac{4\pi^3}{45} g_*(T) \frac{T^4}{M_{\text{Planck}}^2} \,, \tag{B.8}$$

where g_* is the effective number of degrees of freedom

$$g_*(T) = \sum_{\text{bosons}} g_i \left(\frac{T_i}{T}\right)^4 + \frac{7}{8} \sum_{\text{fermions}} g_i \left(\frac{T_i}{T}\right)^4 \,. \tag{B.9}$$

Defining

$$Y = \frac{n}{s} \,, \quad x = \frac{m_S}{T} \tag{B.10}$$

where s is the entropy density

$$s = \frac{2\pi^2}{45} g_{*s}(T) T^3 \,, \tag{B.11}$$

with

$$g_{*s}(T) = \sum_{\text{bosons}} g_i \left(\frac{T_i}{T}\right)^3 + \frac{7}{8} \sum_{\text{fermions}} g_i \left(\frac{T_i}{T}\right)^3 \,, \tag{B.12}$$

the Lee-Weinberg equation (B.1) can be expressed as

$$\frac{\mathrm{d}Y}{\mathrm{d}x} = Z \left(Y^2 - Y_{\text{eq}}^2\right) \,, \tag{B.13}$$

where

$$Z(x) = -\sqrt{\frac{\pi}{45}} \frac{g_*(\frac{m_S}{x})}{\sqrt{g_{*s}(\frac{m_S}{x})}} M_{\text{Planck}} m_S x^{-2} \langle v\sigma \rangle \tag{B.14}$$

and

$$Y_{\text{eq}}(x) = \frac{45}{4\pi^4 g_{*s}(\frac{m_S}{x})} x^2 K_2(x) \,. \tag{B.15}$$

For a given $\langle v\sigma\rangle(x)$ the equation (B.13) can be solved numerically.

However, we may do an approximation which speeds up the calculation preserving good accuracy. We define

$$\delta = \frac{Y}{Y_{\rm eq}} - 1 \tag{B.16}$$

whereby

$$(\delta+1)\frac{\mathrm{d}Y_{\rm eq}}{\mathrm{d}x} + Y_{\rm eq}\frac{\mathrm{d}(\delta+1)}{\mathrm{d}x} = ZY_{\rm eq}^2\delta(\delta+2)\ . \tag{B.17}$$

Now the approximation is that the departure from the equilibrium starts slowly, thus before the freeze out, $x \leq x_f$, we have

$$\frac{\mathrm{d}(\delta+1)}{\mathrm{d}x} = \frac{\mathrm{d}}{\mathrm{d}x}\frac{Y}{Y_{\rm eq}} \approx 0\ . \tag{B.18}$$

Hence

$$\frac{\mathrm{d}Y_{\rm eq}}{\mathrm{d}x} \approx ZY_{\rm eq}^2\frac{\delta(\delta+2)}{\delta+1}\ ,\quad x \leq x_f\ . \tag{B.19}$$

For the numerical solution it is useful to define $y_{\rm eq} = \mathrm{e}^x Y_{\rm eq}$. The equation (B.19) can now be written as

$$x = \ln\left(\frac{Zy_{\rm eq}^2\dfrac{\delta(\delta+2)}{\delta+1}}{\dfrac{\mathrm{d}y_{\rm eq}}{\mathrm{d}x} - y_{\rm eq}}\right)\ . \tag{B.20}$$

Next we pick up a reasonable value for δ_f and solve x_f iteratively from (B.20) . The solution is not very sensitive on the choice of δ and to simplify the equation (B.20) we can choose $\delta = (\sqrt{5}-1)/2$. Moreover we use an approximation

$$\begin{aligned} g_*(T) = & g_{*s}(T) = 2 + 6\cdot\theta(T-M_W) + 3\cdot\theta(T-M_Z) + 3\cdot\frac{7}{4} \\ & + \frac{7}{2}\cdot\sum_{e,\mu,\tau}\theta(T-m_i) + \sum_{\rm scalars} g_i\,\theta(T-m_i) \\ & + \theta(T-T_{\rm QCD})\left(2\cdot 8 + \frac{21}{2}\cdot\sum_{\rm quarks}\theta(T-m_i)\right)\ , \end{aligned} \tag{B.21}$$

which is justified since the in the early universe most of the particles had the same temperature. For the QCD phase transition temperature we use $T_{\rm QCD} = 0.25\,\mathrm{GeV}$.

After the freeze-out, $x > x_f$ we may assume that $Y_{\text{eq}}^2 \ll Y^2$. Hence

$$\frac{\mathrm{d}Y}{\mathrm{d}x} \approx ZY^2 \ , \quad x > x_f \ , \tag{B.22}$$

thus

$$Y(x) = \frac{Y(x_f)}{Y(x_f)A(x,x_f) - 1} \approx \frac{1}{A(x,x_f)}, \tag{B.23}$$

where

$$A(x,x_f) = -\int_{x_f}^{x} Z(x)\mathrm{d}x \ . \tag{B.24}$$

Now the relic abundance is

$$\Omega h^2 = \frac{\rho}{\rho_c} h^2 \ , \tag{B.25}$$

where

$$\begin{aligned} &h = 0.673 \ , \\ &\rho_c = 1.054 \cdot 10^{-5}\, h^2 \ \text{GeV}\,\text{cm}^{-3} \end{aligned} \tag{B.26}$$

are the scale factor for the Hubble expansion rate [8] and the critical density [66], respectively. The WIMP density ρ is

$$\begin{aligned} \rho &= m_S n(x_0) = m_S s(x_0) Y(x_0) \\ &= \frac{2\pi}{45} g_{*s} \left(\frac{m_S}{x_0}\right) \frac{m_S^4}{x_0^3} \frac{1}{A(x_0,x_f)} \ . \end{aligned} \tag{B.27}$$

Now

$$x = x_0 = \frac{m_S}{T_\gamma} \ , \tag{B.28}$$

where $T_\gamma = 2.725\text{K} = 2.348 \cdot 10^{-13}\,\text{GeV}$ is the present day photon temperature [72], so

$$\Omega h^2 = \underbrace{\frac{2\pi}{45} \frac{h^2}{\rho_c} T_\gamma^3 g_{*s}\left(T_\gamma\right)}_{\approx 5.196 \cdot 10^8\ \text{GeV}^{-1}} m_S \left(-\int_{x_f}^{x_0} Z(x)\mathrm{d}x \right)^{-1} \ . \tag{B.29}$$

The Z integral can be evaluated numerically, but with good accuracy it can be approximated as

$$\int_{x_f}^{x_0} Z(x)\mathrm{d}x \approx x_f Z(x_f) \ . \tag{B.30}$$

Appendix C

SS annihilation cross-section

Let us assume, that we have a model which includes three neutral scalar bosons h, H, S and one charged scalar boson H^+ , with interactions described by the Lagrangians

$$\begin{aligned}\mathcal{L}_{\text{scalar}} &= C_1 h S^2 + C_2 h^3 + C_3 h^2 S^2 + C_4 H S^2 + C_5 H h^2 + C_6 H^3 \\ &+ C_7 H^2 S^2 + C_8 h H^2 + C_9 S^2 h H + C_{10} S^2 H^+ H^- + C_{11} h H^+ H^- \\ &+ C_{12} H H^+ H^- \ ,\end{aligned} \tag{C.1}$$

$$\begin{aligned}\mathcal{L}_{\text{gauge}} &= G_1 g^{\mu\nu} h W_\mu^+ W_\nu^- + G_2 g^{\mu\nu} h Z_\mu Z_\nu \\ &+ G_3 g^{\mu\nu} H W_\mu^+ W_\nu^- + G_4 g^{\mu\nu} H Z_\mu Z_\nu \\ &+ G_5 g^{\mu\nu} H^+ H^- W_\mu^+ W_\nu^- \ ,\end{aligned} \tag{C.2}$$

and

$$\mathcal{L}_{\text{fermion}} = F_1 h \psi\overline{\psi} + F_2 H \psi\overline{\psi} \ , \tag{C.3}$$

where C_j, G_j, F_j are the coupling strengths.

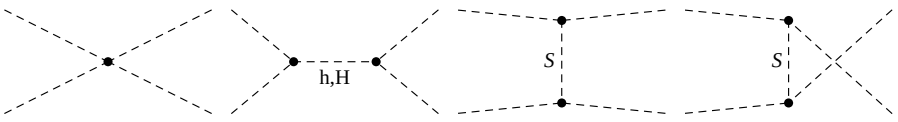

(a) **(b)** **(c)** **(d)**

Figure C.1. Lowest order Feynman diagrams for the annihilation $SS \to hh$.

We would like to calculate the cross-section for the SS annihilation. There are four different two-body final state annihilation channels where the final state particles are scalar bosons:

$$SS \to hh\ ,\ \ SS \to HH\ ,\ \ SS \to hH\ ,\ \ SS \to H^+H^-\ . \tag{C.4}$$

Let us first calculate the cross-section for the annihilation channel $SS \to hh$. The lowest order Feynman diagrams for the annihilation are shown in figure C.1 . Now we may immediately write down the amplitude for the process

$$M_{hh} = \underbrace{4C_3 + 12C_1C_2\frac{1}{s-m_h^2} + 4C_4C_5\frac{1}{s-m_H^2}}_{=A_{hh}} + 2C_1^2\left(\frac{1}{t-m_S^2} + \frac{1}{u-m_S^2}\right)\ . \tag{C.5}$$

The differential cross-section is

$$\frac{\mathrm{d}\sigma_{hh}}{\mathrm{d}t} = \frac{|M_{hh}|^2}{16\pi s(s-4m_S^2)} = \frac{|M_{hh}|^2}{16\pi s^2 v_S^2}\ , \tag{C.6}$$

where

$$v_S^2 = 1 - 4\frac{m_S^2}{s}\ . \tag{C.7}$$

To get σ_{hh} we need to evaluate six integrals. First we need to find out the integration limits. The Mandelstam variable t can be written as

$$t = m_S^2 + m_h^2 - 2E_SE_h + 2|p_S||p_h|\cos\theta \tag{C.8}$$

where the scattering angle θ obtains values from the interval $[0, \pi]$. In the CMS frame

$$|p_S| = \frac{1}{2}\sqrt{s-4m_S^2}\ ,\ \ |p_h| = \frac{1}{2}\sqrt{s-4m_h^2}\ , \tag{C.9}$$

thus the integration limits are

$$t_\pm = \frac{1}{2}\left(2m_S^2 + 2m_h^2 - s \pm \sqrt{s-4m_S^2}\sqrt{s-4m_h^2}\right)\ . \tag{C.10}$$

Evaluating the integrals is rather easy. The integrals are

$$\int_{t_-}^{t_+} \mathrm{d}t = sv_hv_S\ , \tag{C.11}$$

$$\int_{t_-}^{t_+} \mathrm{d}t \frac{1}{u - m_S^2} = \int_{t_-}^{t_+} \mathrm{d}t \frac{1}{t - m_S^2} = \ln \left| 1 - \frac{2sv_h v_S}{s - 2m_h^2 + 2sv_h v_S} \right| \approx -\frac{2sv_h v_S}{s - 2m_h^2} \,, \tag{C.12}$$

$$\begin{aligned} \int_{t_-}^{t_+} \mathrm{d}t \frac{1}{(u - m_S^2)^2} &= \int_{t_-}^{t_+} \mathrm{d}t \frac{1}{(t - m_S^2)^2} \\ &= \frac{4sv_h v_S}{(s - 2m_h^2 - 2sv_h v_S)(s - 2m_h^2 + 2sv_h v_S)} \\ &\approx \frac{4sv_h v_S}{(s - 2m_h^2)^2} \,, \end{aligned} \tag{C.13}$$

$$\begin{aligned} &\int_{t_-}^{t_+} \mathrm{d}t \frac{1}{(t - m_S^2)(u - m_S^2)} \\ &\quad = -\frac{2}{s - 2m_h^2} \ln \left| 1 - \frac{2sv_h v_S}{s - 2m_h^2 + 2sv_h v_S} \right| \\ &\quad \approx \frac{4sv_h v_S}{(s - 2m_h^2)^2} \,, \end{aligned} \tag{C.14}$$

where we have assumed that $s - 2m_h^2 \gg 2sv_h v_S$. If there are two identical bosons in the final state we must take into account symmetry factor $1/2$. Hence the cross-section for the $SS \to hh$ annihilation process is

$$\sigma_{hh} = \frac{v_h}{32\pi v_S s} \left(A_{hh} - 8 \frac{C_1^2}{s - 2m_h^2} \right)^2 \,. \tag{C.15}$$

The $SS \to HH$ process is identical to the $SS \to hh$ process. The annihilation cross-section for the $SS \to HH$ process is

$$\sigma_{HH} = \frac{v_H}{32\pi v_S s} \left(A_{HH} - 8 \frac{C_4^2}{s - 2m_H^2} \right)^2 \,, \tag{C.16}$$

where

$$A_{HH} = 4C_7 + 12C_1 C_8 \frac{1}{s - m_h^2} + 4C_4 C_6 \frac{1}{s - m_H^2} \,. \tag{C.17}$$

Also the $SS \to hH$ channel is similar to the previous channels. The annihilation cross-section for the $SS \to hH$ process is

$$\sigma_{hH} = \frac{v_{hH}}{16\pi v_S s}\left(A_{hH} - 16\frac{C_1 C_4}{s - m_h^2 - m_H^2}\right)^2 , \tag{C.18}$$

where

$$A_{hH} = 2C_9 + 4C_1 C_5 \frac{1}{s - m_h^2} + 4C_4 C_8 \frac{1}{s - m_H^2} , \tag{C.19}$$

and

$$v_{hH}^2 = 1 - \frac{(m_h + m_H)^2}{s} . \tag{C.20}$$

The $SS \to H^+H^-$ channel does not include t and u channel diagrams. The annihilation cross-section for the $SS \to H^+H^-$ process is

$$\sigma_{H^+H^-} = \frac{v_{H^+}}{16\pi v_S s} A_{H^+H^-}^2 , \tag{C.21}$$

where

$$A_{H^+H^-} = 2C_{10} + 2C_1 C_{11} \frac{1}{s - m_h^2} + 2C_4 C_{12} \frac{1}{s - m_H^2} . \tag{C.22}$$

The gauge boson channels include only s channel diagrams with h and H propagators. The Feynman amplitude for the $SS \to W^+W^-$ process is

$$M_{WW} = 4C_1 G_1 \frac{1}{s - m_h^2} \epsilon_1^a \cdot \epsilon_2^a + 4C_4 G_3 \frac{1}{s - m_H^2} \epsilon(k_1, \lambda_1) \cdot \epsilon(k_2, \lambda_2) , \tag{C.23}$$

thus using

$$\sum_{\lambda_j} \epsilon^\mu(k_j, \lambda_j)\epsilon^\nu(k_j, \lambda_j) = -g^{\mu\nu} + \frac{k_j^\mu k_j^\nu}{M_W^2} \tag{C.24}$$

we get

$$|M_{WW}|^2 = 16\left(3 + \frac{s(s - 4M_W^2)}{4M_W^4}\right)\left(\frac{C_1 G_1}{s - m_h^2} + \frac{C_4 G_3}{s - m_H^2}\right)^2 . \tag{C.25}$$

Hence

$$\sigma_{WW} = \frac{v_W}{2\pi v_S s}\left(3 + \frac{s(s - 4M_W^2)}{4M_W^4}\right)\left(\frac{C_1 G_1}{s - m_h^2} + \frac{C_4 G_3}{s - m_H^2}\right)^2 . \tag{C.26}$$

and similarly for the $SS \to ZZ$ process

$$\sigma_{ZZ} = \frac{v_Z}{4\pi v_S s}\left(3 + \frac{s(s - 4M_Z^2)}{4M_Z^4}\right)\left(\frac{C_1 G_2}{s - m_h^2} + \frac{C_4 G_4}{s - m_H^2}\right)^2 . \tag{C.27}$$

Also for the fermionic final states there are only s channel diagrams. The Feynman amplitude for the $SS \to f\overline{f}$ process is

$$M_{ff} = C_1 F_1 \frac{1}{s - m_h^2} \overline{u}(k_1, h_1) v(k_2, h_2) + C_4 F_2 \frac{1}{s - m_H^2} \overline{u}(k_1, h_1) v(k_2, h_2) \tag{C.28}$$

Making use of identities

$$\begin{aligned} \sum_{h_1} u(k_1, h_1)\overline{u}(k_1, h_1) &= \not{k}_1 + m_f \ , \\ \sum_{h_2} v(k_2, h_2)\overline{v}(k_2, h_2) &= \not{k}_2 - m_f \ , \end{aligned} \tag{C.29}$$

and

$$\mathrm{Tr}(\not{k}_1 \not{k}_2) = 4 k_1 \cdot k_2 \ , \tag{C.30}$$

we get

$$|M_{ff}|^2 = 2 N_C s (s - 4m_f^2) \left(C_1 F_1 \frac{1}{s - m_h^2} + C_4 F_2 \frac{1}{s - m_H^2} \right)^2 \ , \tag{C.31}$$

where $N_C = 1$ for leptons and $N_C = 3$ for quarks. Hence

$$\sigma_{ff} = \frac{N_C v_f}{16 \pi v_S s} (s - 4m_f^2) \left(C_1 F_1 \frac{1}{s - m_h^2} + C_4 F_2 \frac{1}{s - m_H^2} \right)^2 \ . \tag{C.32}$$

Bibliography

[1] J. J. Aubert, U. Becker *et. al.*, *Phys.Rev.Lett.* **33** (1974) 1404.

[2] S. Herb, D. Hom, L. Lederman, J. Sens, H. Snyder *et. al.*, *Phys.Rev.Lett.* **39** (1977) 252.

[3] **CDF** collaboration, F. Abe, H. Akimoto, Akopian *et. al.*, *Phys.Rev.Lett.* **74** (1995) 2626.

[4] **UA1** collaboration, G. Arnison *et. al.*, *Phys.Lett.* **B126** (1983) 398.

[5] **UA1** collaboration, G. Arnison *et. al.*, *Phys.Lett.* **B122** (1983) 103.

[6] **ATLAS** collaboration, 2012. ATLAS-CONF-2012-091.

[7] **CMS** collaboration, S. Chatrchyan *et. al.*, *Phys.Lett.* **B716** (2012) [arXiv:1207.7235 [hep-ex]].

[8] **Planck** collaboration, P. Ade *et. al.*, arXiv:1303.5076 [astro-ph.CO].

[9] S. Weinberg, *Phys.Rev.Lett.* **19** (1967) 1264.

[10] S. Glashow, *Nucl.Phys.* **22** (1961) 579.

[11] P. W. Higgs, *Phys.Rev.Lett.* **13** (1964) 508.

[12] C. Guralnik, G.S. Hagen and T. Kibble, *Advances in Physics* **2** (1967) .

[13] **CDF, D0** collaboration, T. Aaltonen *et. al.*, *Phys.Rev.Lett.* **109** (2012) 071804 [arXiv:1207.6436 [hep-ex]].

[14] **ATLAS** collaboration, 2012. ATLAS-CONF-2012-170.

[15] **CMS** collaboration, 2013. CMS-PAS-HIG-13-005.

[16] A. Schaffer, arXiv:1301.2802 [hep-ex].

[17] **LHC Higgs Cross Section Working Group** collaboration, S. Dittmaier *et. al.*, arXiv:1101.0593 [hep-ph].

[18] **Tevatron New Phenomena and Higgs Working Group** collaboration, Tevatron New Physics Higgs Working Group and CDF and D0 collaborations, arXiv:1207.0449 [hep-ex].

[19] **LHC Higgs Cross Section Working Group** collaboration, S. Dittmaier *et. al.*, arXiv:1201.3084 [hep-ph].

[20] **Atlas** collaboration, 2013. ATLAS-CONF-2013-034.

[21] P. P. Giardino, K. Kannike, I. Masina, M. Raidal and A. Strumia, arXiv:1303.3570 [hep-ph].

[22] J. Espinosa, C. Grojean, M. Muhlleitner and M. Trott, *JHEP* **1212** (2012) 045 [arXiv:1207.1717 [hep-ph]].

[23] D. Carmi, A. Falkowski, E. Kuflik, T. Volansky and J. Zupan, *JHEP* **1210** (2012) 196 [arXiv:1207.1718 [hep-ph]].

[24] A. Celis, V. Ilisie and A. Pich, arXiv:1302.4022 [hep-ph].

[25] T. Alanne, S. Di Chiara and K. Tuominen, arXiv:1303.3615 [hep-ph].

[26] J. Gunion, H. Haber, G. Kane and S. Dawson, *The Higgs Hunter's Guide*. Frontiers in Physics. Perseus Publishing, 2000.

[27] G. Bertone, D. Hooper and J. Silk, *Phys.Rept.* **405** (2005) 279 [arXiv:hep-ph/0404175 [hep-ph]].

[28] G. Jungman, M. Kamionkowski and K. Griest, *Phys.Rept.* **267** (1996) 195 [arXiv:hep-ph/9506380 [hep-ph]].

[29] J. M. Cline, arXiv:hep-ph/0609145 [hep-ph].

[30] C. T. Hill and E. H. Simmons, *Phys.Rept.* **381** (2003) 235 [arXiv:hep-ph/0203079 [hep-ph]].

[31] J. D. Wells, arXiv:0909.4541 [hep-ph].

[32] E. Farhi and L. Susskind, *Phys.Rept.* **74** (1981) 277.

[33] F. Zwicky, *Astrophys. J.* **86** (1937) 217.

[34] T. van Albada, J. N. Bahcall, K. Begeman and R. Sancisi, *Astrophys.J.* **295** (1985) 305.

[35] R. H. Sanders and S. S. McGaugh, *Ann.Rev.Astron.Astrophys.* **40** (2002) 263 [arXiv:astro-ph/0204521 [astro-ph]].

[36] D. Clowe, M. Bradac, A. H. Gonzalez, M. Markevitch, S. W. Randall *et. al.*, *Astrophys.J.* **648** (2006) L109 [arXiv:astro-ph/0608407 [astro-ph]].

[37] **WMAP** collaboration, C. Bennett *et. al.*, arXiv:1212.5225 [astro-ph.CO].

[38] B. Patt and F. Wilczek, arXiv:hep-ph/0605188 [hep-ph].

[39] A. Djouadi, O. Lebedev, Y. Mambrini and J. Quevillon, *Phys.Lett.* **B709** (2012) 65 [arXiv:1112.3299 [hep-ph]].

[40] **XENON100** collaboration, E. Aprile *et. al.*, *Phys.Rev.Lett.* **109** (2012) 181301 [arXiv:1207.5988 [astro-ph.CO]].

[41] **IceCube** collaboration, M. Aartsen *et. al.*, *Phys.Rev.Lett.* **110** (2013) 131302 [arXiv:1212.4097 [astro-ph.HE]].

[42] A. G. Cohen, A. De Rujula and S. Glashow, *Astrophys.J.* **495** (1998) 539 [arXiv:astro-ph/9707087 [astro-ph]].

[43] **WMAP** collaboration, E. Komatsu *et. al.*, *Astrophys.J.Suppl.* **192** (2011) 18 [arXiv:1001.4538 [astro-ph.CO]].

[44] A. Sakharov, *Pisma Zh.Eksp.Teor.Fiz.* **5** (1967) 32.

[45] M. Fukugita and T. Yanagida, *Phys.Lett.* **B174** (1986) 45.

[46] M. Yoshimura, *Phys.Rev.Lett.* **41** (1978) 281.

[47] V. Rubakov and M. Shaposhnikov, *Usp.Fiz.Nauk* **166** (1996) 493 [arXiv:hep-ph/9603208 [hep-ph]].

[48] S. Davidson, E. Nardi and Y. Nir, *Phys.Rept.* **466** (2008) 105 [arXiv:0802.2962 [hep-ph]].

[49] A. Riotto and M. Trodden, *Ann.Rev.Nucl.Part.Sci.* **49** (1999) 35 [arXiv:hep-ph/9901362 [hep-ph]].

[50] M. Kobayashi and T. Maskawa, *Prog.Theor.Phys.* **49** (1973) 652.

[51] M. Gavela, P. Hernandez, J. Orloff, O. Pene and C. Quimbay, *Nucl.Phys.* **B430** (1994) 382 [arXiv:hep-ph/9406289 [hep-ph]].

[52] K. Kajantie, M. Laine, K. Rummukainen and M. E. Shaposhnikov, *Phys.Rev.Lett.* **77** (1996) 2887 [arXiv:hep-ph/9605288 [hep-ph]].

[53] J. McDonald, *Phys.Rev.* **D50** (1994) 3637 [arXiv:hep-ph/0702143 [hep-ph]].

[54] J. M. Cline and K. Kainulainen, *JCAP* **1301** (2013) 012 [arXiv:1210.4196 [hep-ph]].

[55] J. M. Cline, K. Kainulainen, P. Scott and C. Weniger, arXiv:1306.4710 [hep-ph].

[56] B. W. Lee and S. Weinberg, *Phys.Rev.Lett.* **39** (1977) 165.

[57] I. F. Ginzburg and M. Krawczyk, *Phys.Rev.* **D72** (2005) 115013 [arXiv:hep-ph/0408011 [hep-ph]].

[58] H. Haber, G. L. Kane and T. Sterling, *Nucl.Phys.* **B161** (1979) 493.

[59] J. F. Donoghue and L.-F. Li, *Phys.Rev. D* **19** (1979) 945.

[60] T. P. Cheng and M. Sher, *Phys.Rev. D* **35** (1987) 3484.

[61] P. Ferreira, R. Santos and A. Barroso, *Phys.Lett.* **B603** (2004) 219 [arXiv:hep-ph/0406231 [hep-ph]].

[62] I. Ginzburg and I. Ivanov, *Phys.Rev.* **D72** (2005) 115010 [arXiv:hep-ph/0508020 [hep-ph]].

[63] A. G. Akeroyd, A. Arhrib and E.-M. Naimi, *Phys.Lett.* **B490** (2000) 119 [arXiv:hep-ph/0006035 [hep-ph]].

[64] M. E. Peskin and T. Takeuchi, *Phys.Rev.* **D46** (1992) 381.

[65] I. Maksymyk, C. Burgess and D. London, *Phys.Rev.* **D50** (1994) 529 [arXiv:hep-ph/9306267 [hep-ph]].

[66] **Particle Data Group** collaboration, J. Beringer *et. al.*, *Phys.Rev.* **D86** (2012) 010001.

[67] W. Grimus, L. Lavoura, O. Ogreid and P. Osland, *Nucl.Phys.* **B801** (2008) 81 [arXiv:0802.4353 [hep-ph]].

[68] **ALEPH** collaboration, A. Heister *et. al.*, *Phys.Lett.* **B543** (2002) 1 [arXiv:hep-ex/0207054 [hep-ex]].

[69] **CMS** collaboration, S. Chatrchyan *et. al.*, *Phys.Lett.* **B710** (2012) 26 [arXiv:1202.1488 [hep-ex]].

[70] T. Alanne, J. M. Cline, K. Kainulainen, K. Tuominen and V. Vaskonen, work in progress.

[71] P. Gondolo and G. Gelmini, *Nucl.Phys.* **B360** (1991) 145.

[72] D. Fixsen, *Astrophys.J.* **707** (2009) 916 [arXiv:0911.1955 [astro-ph.CO]].